OUTCROP CHEMOSTRATIGRAPHIC CORRELATION OF THE UPPER GREEN RIVER FORMATION IN THE UINTA BASIN, UTAH— MAHOGANY OIL SHALE ZONE TO THE UINTA FORMATION

by Dave Keighley

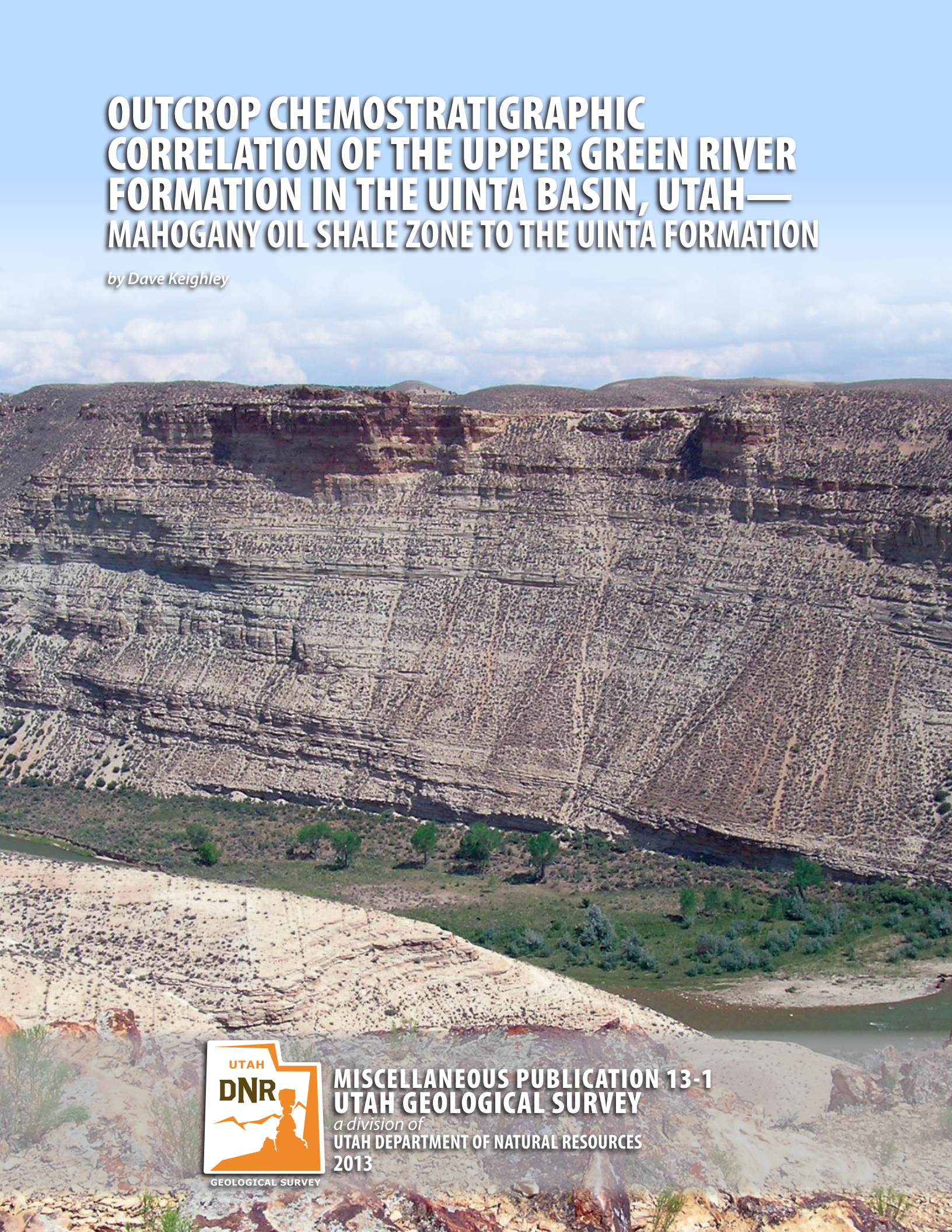

UTAH DNR GEOLOGICAL SURVEY

MISCELLANEOUS PUBLICATION 13-1
UTAH GEOLOGICAL SURVEY
a division of
UTAH DEPARTMENT OF NATURAL RESOURCES
2013

OUTCROP CHEMOSTRATIGRAPHIC CORRELATION OF THE UPPER GREEN RIVER FORMATION IN THE UINTA BASIN, UTAH— MAHOGANY OIL SHALE ZONE TO THE UINTA FORMATION

by Dave Keighley, PhD, P.G.

Department of Earth Sciences
University of New Brunswick
Fredericton, Canada

ISBN: *978-1-55791-875-8*

Cover photo: *White River near Cowboy Canyon, eastern Uinta Basin, Utah.*

MISCELLANEOUS PUBLICATION 13-1
UTAH GEOLOGICAL SURVEY
a division of
UTAH DEPARTMENT OF NATURAL RESOURCES
2013

STATE OF UTAH
Gary R. Herbert, Governor

DEPARTMENT OF NATURAL RESOURCES
Michael Styler, Executive Director

UTAH GEOLOGICAL SURVEY
Richard G. Allis, Director

PUBLICATIONS
contact
Natural Resources Map & Bookstore
1594 W. North Temple
Salt Lake City, UT 84116
telephone: 801-537-3320
toll-free: 1-888-UTAH MAP
website: mapstore.utah.gov
email: geostore@utah.gov

UTAH GEOLOGICAL SURVEY
contact
1594 W. North Temple, Suite 3110
Salt Lake City, UT 84116
telephone: 801-537-3300
website: geology.utah.gov

CONTENTS

ABSTRACT 1
INTRODUCTION 1
LITHOSTRATIGRAPHY 2
METHODS 5
SEDIMENTOLOGICAL LOGS 10
Gate Canyon 10
Buck Canyon 10
Cowboy Canyon 11
Potential Correlations 12
ICP RESULTS SUMMARY 12
Review of Previously Analyzed Data from Buck Canyon 12
New ICP Data: Gate, Buck, and Cowboy Canyons 12
Data Collection Summary 12
Anomalous Elemental Peaks: Phosphorus 15
Anomalous Elemental Peaks: Uranium, Thorium, Strontium, Barium 17
Anomalous Elemental Peaks: Rare Earth Elements 17
Anomalous Elemental Peaks: Other Elements 17
PAAS-Normalized Spider Plots: REEs 19
General Depth Trends 20
Geochemical Correlation 23
XRD RESULTS SUMMARY 23
SEM RESULTS SUMMARY 24
DISCUSSION 24
CONCLUSIONS 26
ACKNOWLEDGMENTS 28
REFERENCES 28
APPENDICES ..... on CD
Appendix I: Tabulated ICP Results ..... on CD
Appendix II: Gate Canyon – Elemental Abundance verses Elevation ..... on CD
Appendix III: Buck Canyon – Elemental Abundance verses Elevation ..... on CD
Appendix IV: Cowboy Canyon – Elemental Abundance verses Elevation ..... on CD
Appendix V: Gate Canyon – Spider Plots of REE Abundance verses PAAS ..... on CD
Appendix VI: Buck Canyon – Spider Plots of REE Abundance verses PAAS ..... on CD
Appendix VII: Cowboy Canyon – Spider Plots of REE Abundance verses PAAS ..... on CD
Appendix VIII: XRD Analyses ..... on CD

FIGURES

Figure 1. General location map 2
Figure 2. General geological maps 3
Figure 3 General surface lithostratigraphic terminology for the lacustrine phases of the Uinta Basin 4
Figure 4. Summary sedimentary logs of outcropping upper Green River Formation strata at Buck, Gate, and Cowboy Canyons 7
Figure 5. Potential correlations of strata at Buck, Gate, and Cowboy Canyons 13
Figure 6. Summary statistics of the rare earth elements 15
Figure 7. Ratio-elevation plots for silicon against selected elements at Buck, Gate, and Cowboy Canyons 16
Figure 8. Scatter plots of elements P, La, Th, and U 18
Figure 9. Summary statistics of the rare earth elements at Buck, Gate, and Cowboy Canyons 19
Figure 10. Selected spider plots of phosphatic oil shale samples at Buck, Gate, and Cowboy Canyons 20
Figure 11. Ratio-elevation plots at Buck, Gate, and Cowboy Canyons 21
Figure 12. Selected REE spider plots of tuff and tuffaceous sandstone samples at Buck, Gate, and Cowboy Canyons 24
Figure 13. X-ray diffractometer traces of selected samples from Buck Canyon 25
Figure 14. SEM images of a bedding surface in the oil shale at 128.2 m in the Buck Canyon section 26
Figure 15. The phosphorus cycle in lakes. 27
Figure 16. Currently preferred correlation of strata at Buck, Gate, and Cowboy Canyons 27

TABLES

Table 1. Broad lithofacies classification for Gate, Buck, and Cowboy Canyons 6
Table 2. List of elements analyzed by ICP methods 9

OUTCROP CHEMOSTRATIGRAPHIC CORRELATION OF THE UPPER GREEN RIVER FORMATION IN THE UINTA BASIN, UTAH— MAHOGANY OIL SHALE ZONE TO THE UINTA FORMATION

by Dave Keighley

ABSTRACT

The Green River Formation of the Uinta Basin in eastern Utah is host to not only one of the world's largest oil shale deposits, primarily in the Mahogany oil shale zone, but it also contains significant conventional oil and gas reserves in interfingering sand bodies that grade into the laterally equivalent Colton and Wasatch Formations. However, very few marker beds and intervals can be correlated across the basin to help subdivide the 2 km-thick succession of upper Green River Formation strata overlying the main oil shale zone. This report forms part of an ongoing attempt to subdivide this sedimentary succession by identifying systematic variations in the abundance of particular elements, by way of inductively coupled plasma (ICP) spectrometry analyses, to produce a chemostratigraphy of the succession.

Rock samples, ascribed to one of four broad lithotypes (tuff, sandstone, oil shale, or most commonly, variably marly and shaley mudstone), were collected at logged sections from Gate Canyon, Buck Canyon, and Cowboy Canyon, west to east, along the southern limb of the Uinta Basin. ICP spectrometry of samples from several of the oil shale beds displays anomalously high abundances of phosphorus, in combination with elevated uranium, and rare-earth elements. A phosphorus content of between 6.0 and 7.5 wt %, along with a gradual enrichment progressively from the light to heavy rare-earth elements, is recorded in oil shale both at Buck Canyon (128.2 m above base Mahogany oil shale zone) and Cowboy Canyon (124.8 m above base Mahogany), allowing for their correlation. Two other phosphatic oil-shale beds also can be correlated between two of the three studied localities based on differing patterns of REE enrichment. These phosphorus and associated uranium and rare-earth anomalies are considered related to the production, just below the sediment-water interface, of very early diagenetic calcium fluorapatite that was able to fossilize coccoid microbes under reducing conditions. Collectively, these anomalies can reasonably be equated to depositional time-lines. This correlation scheme suggests a significant thickening of the succession to the west of the study area, toward Gate Canyon. Correlation of sandstone, tuff, and tuffaceous sandstone also holds promise, but to date is less convincing. However, rare-earth compositions of such samples also tend to support the aforementioned correlation.

A stratigraphically abrupt reduction upsection in the magnesium-calcium ratio is also identified at different stratigraphic positions in Gate Canyon (195 m) and Buck Canyon (75 m). Values in Cowboy Canyon suggest that at this location the abrupt reduction would have to occur below the Mahogany oil shale zone. The magnesium-calcium boundary therefore crosses established stratigraphic surfaces and so must be considered a later, diagenetic feature, probably related to deep burial or pre-uplift (de-) dolomitization, and thus a boundary that can cross time lines and marker beds.

INTRODUCTION

The Paleogene Green River Formation (GRF) of Utah, Colorado, and Wyoming (figure 1) is classified as the world's largest oil shale deposit, estimated at over 2.85 trillion barrels of oil in place (Johnson and others, 2010). In the Uinta Basin of eastern Utah (figure 2), the GRF is also host to conventional oil and gas reserves (450 MMBO produced; Morgan and others, 2002) present in interfingering sand bodies that grade into the laterally equivalent Colton and Wasatch Formations (figure 3). However, in the central part of the Uinta Basin, carbonate mudstone and shale of the GRF and overlying lower Uinta Formation attains a thickness of ~2,200 m (7,200 ft; Picard, 1957) yet there are very few marker beds and intervals that can be correlated across the Basin (cf. Ruble and Philp, 1998, their figure 3) to help stratigraphically subdivide the succession. The lack of regional extent means that the relative positions of these marker beds to each other and to potential petroleum-reservoir sandstone beds (e.g., interfingering basal Uinta Formation sandstone) in the subsurface remains tentative at the larger basin-wide scale. As an example, for much of the succession it is not currently possible to accurately determine how a thick package of mudstone in the central part of the basin correlates laterally to the east with another mudstone package lying above or below an interfingering sandstone of the Uinta Formation, or Wasatch Formation.

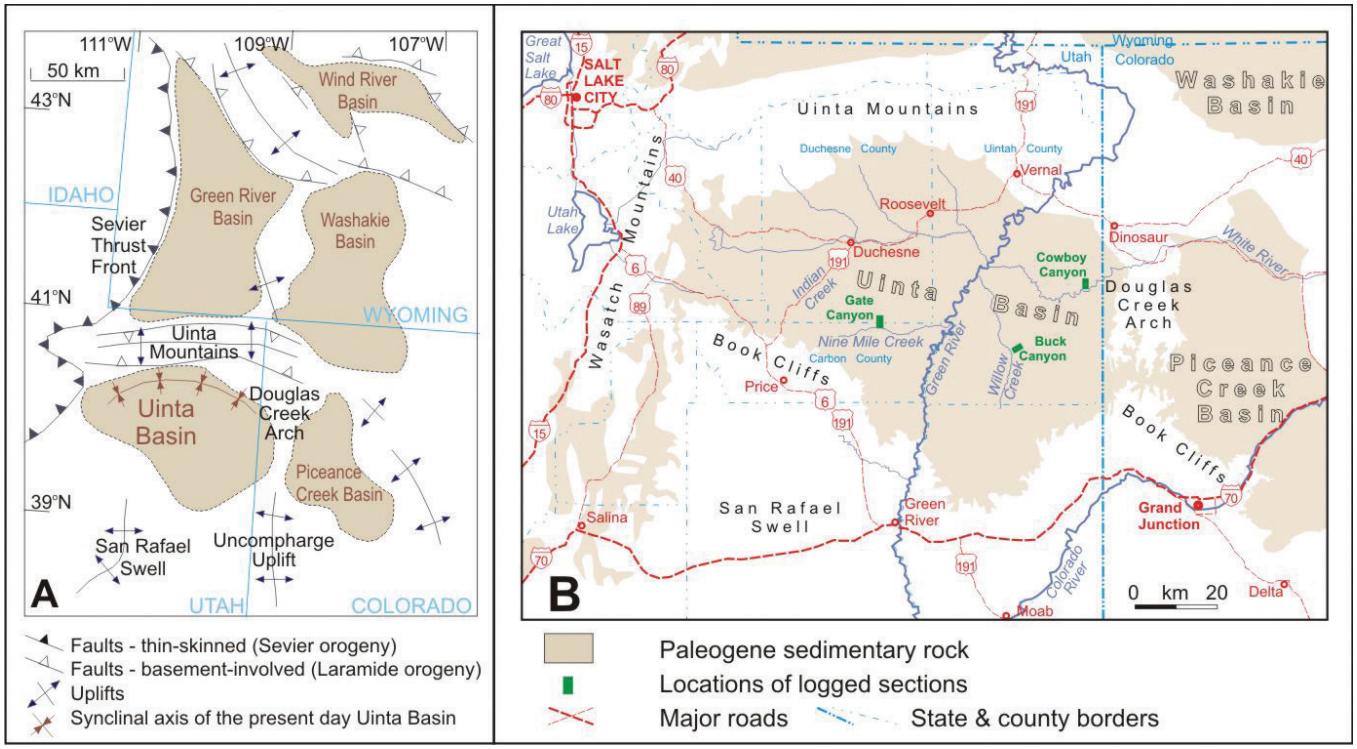

***Figure 1**. (A) General location map of the major Laramide basins in western United States (after Dickinson et al., 1988). (B) Political and road map for the Uinta Basin.*

Elsewhere, similar thick, homogenous sedimentary successions that lack biostratigraphic markers or control have now been subdivided based on their elemental signatures (e.g., Ehrenberg and Siring, 1992; Racey and others, 1995; Wray, 1999; Pearce and others, 1999, 2008; Ratcliffe and others, 2004, 2006). This chemostratigraphic approach identifies systematic variation in the abundance of particular elements usually by way of various inductively coupled plasma (ICP) spectrometry or X-ray fluorescence (XRF) analyses of samples from a vertical succession.

An earlier unpublished project for the Utah Geological Survey had included ICP analysis for the purpose of recording elemental abundance of samples collected by a student in a logged section north of Buck Canyon in the Uinta Basin. This initial work indicated that the sedimentary succession of the GRF, from the top of the Mahogany oil shale zone (MOSZ) up into the basal interval of the Uinta Formation, could potentially be subdivided by its elemental geochemistry. In other words, a chemostratigraphy for the upper member might be possible based on the identification of beds with unique elemental anomalies, gradual or stepped trends of increasing/decreasing elemental ratios in particular intervals of the succession, or changing dispersion about the mean of the ratio at particular horizons.

This paper reports on the current state of investigations into the potential for chemostratigraphic subdivision of the upper GRF using data from ICP analyses undertaken for the author by Activation Laboratories, Canada (Actlabs), with additional information derived from in-house (University of New Brunswick, Canada) XRD and scanning electron microscopy (SEM) analyses.

LITHOSTRATIGRAPHY

A typical lacustrine, tripartite vertical succession (Lambiase, 1990) is identified in the Paleocene–Eocene of the Uinta Basin (figure 3). At the base, a gray to red conglomerate, sandstone, and mudstone succession is described as the Wasatch Formation eastward of the Green River. West of the river, these mostly coarse-grained clastics comprise a basal North Horn Formation and an overlying Colton Formation, interpreted to be the initial alluvial inputs into the developing basin. These latter two formations are typically separated by an interfingering carbonate, the Flagstaff Limestone, representing an early lacustrine phase. This carbonate unit is considered mostly of Paleocene age and has been considered both a separate formation (e.g., Witkind, 1995) and a basal member of the GRF (e.g., Ruble and Philp, 1998).

Progressively upsection, variably shaley, variably carbonate-, evaporite-, and organic-rich mudstone, assigned to the GRF, cyclically onlap toward the basin margin as the basin continued to deepen and the lake fluctuated, but generally expanded in size. Oil shale is present at various levels within the GRF, but the richest beds are concentrated within an approximately 30 m-thick interval collectively termed the Mahogany oil shale zone (MOSZ), which in-

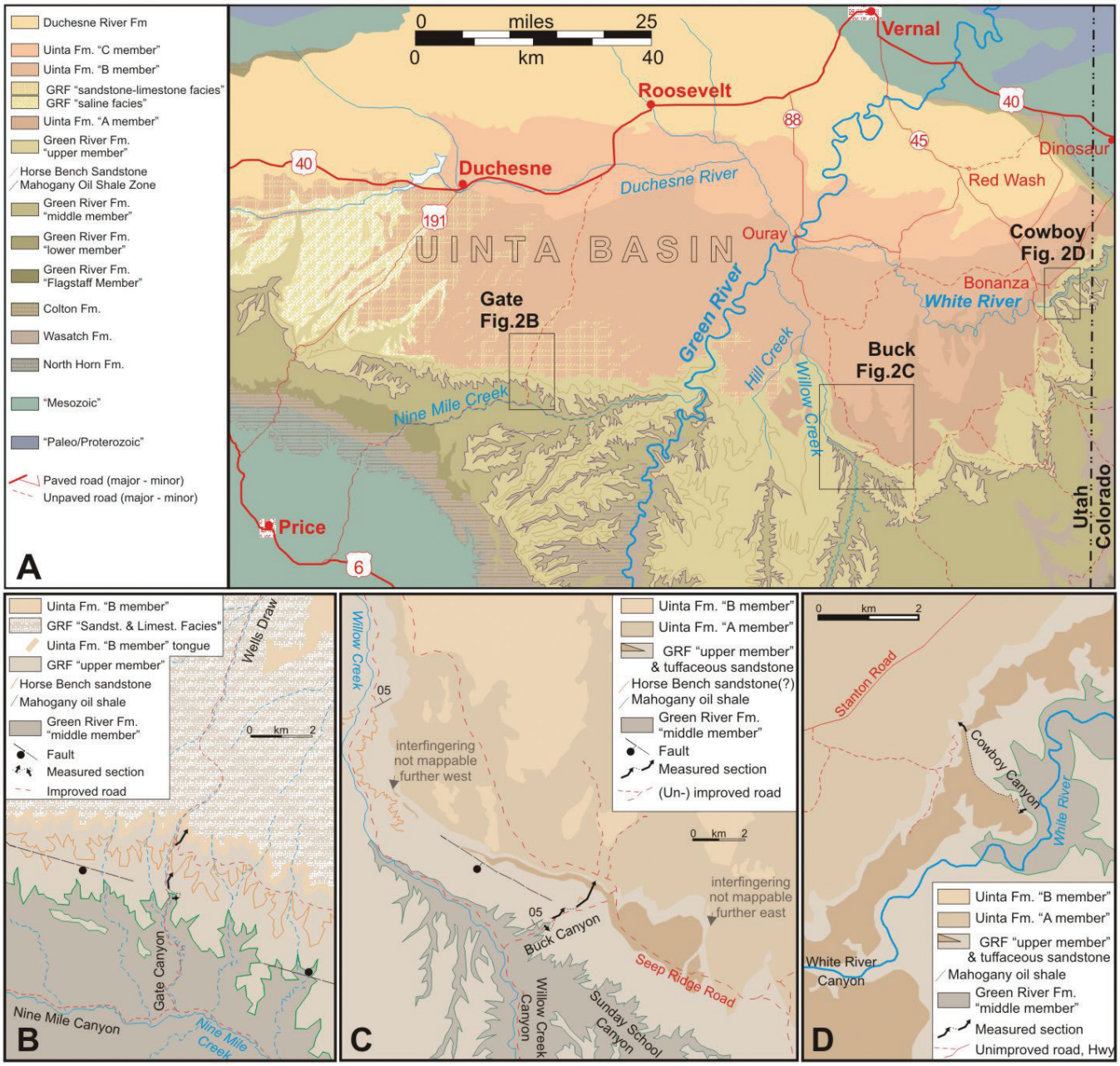

***Figure 2**. Geological maps of the (A) Uinta Basin and adjacent basins, including the location of the logged and sampled sections at (B) Gate Canyon, (C) Buck Canyon, and (D) Cowboy Canyon. Modified from Rowley and others, 1985; Gualtieri, 1988; Witkind, 1988, 1995; Weiss and others, 1990; Bryant, 1992; and Sprinkel, 2009.*

cludes, in outcrop, the Mahogany ledge that itself contains the ≤1.5 m-thick Mahogany oil shale bed (Cashion, 1967). The MOSZ is considered to mark the base of the informal upper member of the GRF (Weiss and others, 1990; Morgan and others, 2002; henceforth "upper GRF") and the zone is one of the most widely correlated marker units, being traceable across most of the Uinta Basin and eastward into the Piceance Creek Basin of Colorado. An alternative, more formal lithostratigraphy persists east of the Green River toward the basin center, where several alternating organic-rich and organic-poor carbonate mudstone intervals are distinctive below the MOSZ. These beds, together with the overlying variably marly, tuffaceous, and shaley mudstone, oil shale and tuff elsewhere included in the upper GRF, are mapped as the Parachute Creek Member (Cashion and Donnell, 1974; Sprinkel, 2009). Uinta-, and other Laramide-basin oil shale has previously been interpreted as having formed in playa-lake conditions, stratified deep-water conditions or, possibly some in deep, some in shallow (e.g., Bradley and Eugster, 1969; Bradley, 1973; Eugster and Hardie, 1975; Surdam and Wolfbauer, 1975; Desborough, 1978; Boyer, 1982). Current consensus has the MOSZ representing deposition during the most prolonged extent of merged lakes that periodically filled both depressions ("Lake Uinta"; e.g., Cashion, 1967; Keighley and others, 2003b), and which are correlated by

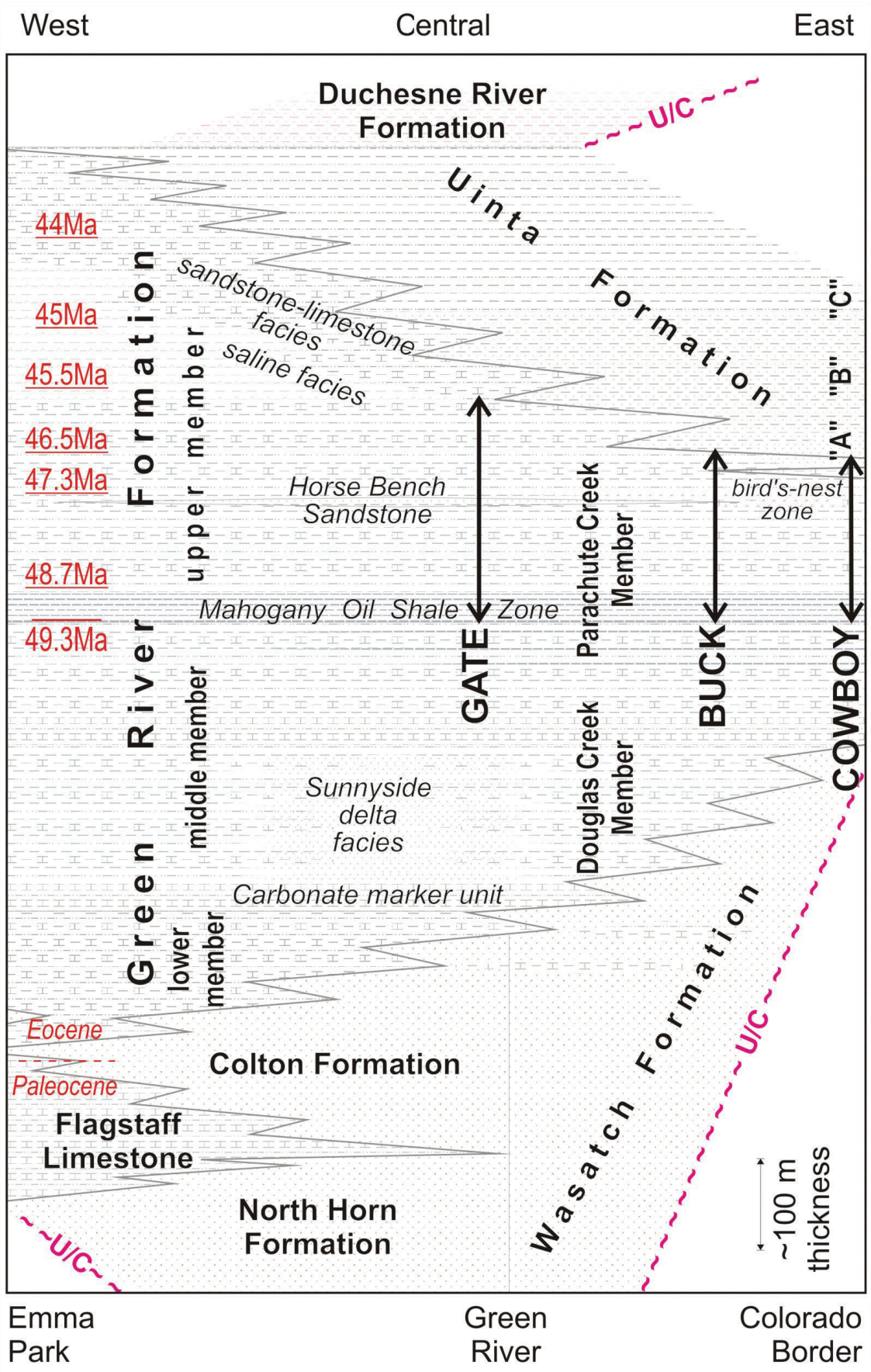

***Figure 3**. General surface lithostratigraphic terminology for the lacustrine phases of the Uinta Basin. Approximate radiometric ages from tuff beds (Smith and others, 2008; Birgenheier and Vanden Berg, 2011) shown in red.*

Birgenheier and Vanden Berg (2011) to deposition following the Early Eocene Climatic Optimum.

The upper GRF contains, most prominently west of the Green River and ~150 m above the MOSZ (Dane, 1955; Remy, 1992), the Horse Bench Sandstone (HBS), which used to be considered the base of the now-abandoned "Evacuation Creek Member" (Cashion and Donnell, 1974). In Willow Creek, the HBS is much thinner and lies ~120 m above the MOSZ (figure 3); it is increasingly difficult to trace farther eastward. Another regionally restricted marker interval is present southeast of Bonanza. In the basal part of the Evacuation Creek Member, Cashion (1967) identified an interval with many (in outcrop, leached or altered to calcite) nahcolite ($NaHCO_3$) nodules, that he informally termed the "bird's-nest zone" (note that, herein, the "Bird's Nest Saline Zone", or BNSZ, is used for evaporitic beds considered to be at a similar stratigraphic position). Nodular textures have also been identified in the nearby P4 core, as well as northwest toward the basin center (Birgenheier and Vanden Berg, 2011). The exact correlation of this saline interval to the HBS has not been conclusively demonstrated, but Dyni (2008) appears to consider the two units laterally equivalent.

Interbedded sandstone and mudstone of the Uinta Formation progressively caps the upper GRF, the contact being stratigraphically higher in the west than the east (Cashion, 1967). This is due to pinch-outs of medium- to fine-grained sandstone (characteristic of the informal "A" member of the Uinta Formation), which represent fluvial-deltaic deposits that gradually infilled both the Piceance Creek Basin and then the Uinta Basin from the northeast (Johnson, 1981; Donnell, 2009). To the west and upsection, finer grained sandstone and variegated mudstone (Uinta Formation, member "B") interfingers with a >500 m succession of mudstone, limestone, and yet more evaporite beds known as the "saline facies" and "sandstone and limestone facies" (e.g., Keighley and others, 2003a). Near Duchesne, boreholes intersecting these facies contain numerous sodic salts (Dyni, 1996), indicating that the lake eventually evolved from brackish into a hypersaline system (Smith and others, 2008). Although included as part of the Uinta Formation by Dane (1954) these facies intervals, along with thin tongues of Uinta Formation-type sandstone, have been included by subsequent workers as part of the upper GRF (figure 3).

Several tuff beds are also present in the upper GRF. Near the base of, and slightly above the MOSZ, respectively, are the "Curly" and "Wavy" tuff beds that are considered traceable from Gate Canyon (Remy, 1992) east into the Piceance Creek Basin (Smith and others, 2008). The "Mahogany" tuff additionally forms, locally, part of the MOSZ. Overlying named and dated tuff are, successively, the "Blind Canyon", "Fat", "Portly", "Oily", and "Strawberry" tuffs. It is uncertain whether the latter four have been correlated any farther east than Indian Canyon. Smith and others (2008) also demarcate a volcaniclastic basal Uinta Formation that extends west from the Piceance Creek Basin into the Uinta Basin. In outcrop, volcaniclastic sandstone displays a highly variable weathering signature making mapping and correlation difficult: sometimes cliff-, ledge-, or slope-forming, sometimes a distinct orange, brown, or pale yellow color. At Willow Creek, Sprinkel (2008) maps a westward pinch-out of a tuffaceous/volcaniclastic sandstone as a basal interfingering of Uinta Formation into the upper GRF (figure 2D). However, further east it is uncertain as to whether the presence of tuffaceous sandstone outcrops represents (i) westward pinch-outs of additional, underlying volcaniclastic tongues or that (ii) such outcrops correlate laterally with the Willow Creek volcaniclastic sandstone and represent a distinct unit beneath the base of the Uinta Formation.

METHODS

Sections through the upper GRF were logged and sampled at, from west to east, Gate, Buck, and Cowboy Canyons on the southern limb of the Uinta Basin (figure 2), representing a transect parallel then oblique to depositional strike and gradually basinward toward the east. All logged and sampled material can be ascribed to one of four broad lithotypes: oil shale, carbonate mudstone, sandstone, and tuff, although considerable variation is present in each, including material nearly intermediate between the aforementioned four end members (table 1). Most commonly sampled was the variably shaley, carbonate-rich mudstone which is predominant throughout the upper GRF. This lithotype is often badly weathered and so typically poorly exposed, particularly in the interval just above the MOSZ, where systematic sampling described below is most challenging. Here, an interval of poor exposure is often reflected in very gentle, soil-covered slopes, which limits the precise measurement of vertical thickness. Where the mudstone is interbedded with more resistant, thin (<0.1 m) tuff units and oil shale, minor ledges often form. Ledges of sandstone, interbedded with mudstone or uncommon tuff, attain thicknesses of up to 5 m.

In a previous unpublished study for the Utah Geological Survey, 51 samples were collected for analysis from Buck Canyon, at approximately 3 m intervals, from above the poorly exposed interval up to the first interfingering of the Uinta Formation (additional samples from the overlying strata were also measured). Due to concerns over the original measurement of this section, and thus the actual location of the sampled horizons, the Buck Canyon section was relogged for this report. The sampling program for this project involved systematic collection of rock at a 4 m (vertical thickness) sampling interval in all three canyons. If there was no rock exposed at the required stratigraphic elevation, a sample was taken from the nearest outcrop,

***Table 1**. Broad lithofacies classification for Gate, Buck, and Cowboy Canyons.*

Lithofacies	Description	Interpretation	Occurrence
1. Oil shale	Beds typically between 10 and 150 mm thick, purplish-black, to brown to dark gray, micro-laminated to massive, often within one bed. Hard, light-gray weathering, slightly domal crusts (?algal) rarely cap the beds. Rarely, 2 mm angular crystals of (?pseudomorphing) carbonate are interspersed in very finely laminated beds. Interbedded and gradational with lithofacies 2, rarely with 4.	Lacustrine low energy under eutrophic conditions	Rare. Most common, 0-35 m (MOSZ) in all sections, sporadic up to 190 m at Gate, up to 145 m at Buck, and up to the base Uinta Formation at Cowboy.
2. Mudstone	Mudstone, often marly to variably calcareous/dolomitic, micro-laminated to apparently massive, can be variably colored (e.g., brown, olive, greenish gray, mid to light gray, and buff), variably arenaceous and silty, and variably tuffaceous. Commonly extensive soft-sediment deformation, rarely with diastasis cracks and rusted (altered) pyrite nodules. Lamination highly disrupted in rare intervals with abundant evaporite (nahcolite) crystals. Interbedded and gradational with all other lithofacies.	Lacustrine offshore and low energy nearshore with possible rare exposed mudflat and paleosol	Predominant throughout.
3. Sandstone	Beds generally thin, tabular, and very fine grained, buff, brown, orange, or yellowish gray in color and variably calcareous. Lateral and vertical stacking of lenticular beds occurs in fine-medium grained sandstone of the basal Uinta A. Sedimentary structures include asymmetric ripple cross-lamination, low-angle and planar cross-bedding, and soft-sediment deformation structures. Included in this lithofacies are very rare, thin mud-pebbly sandstone lenses (Gate Canyon only). Interbedded and gradational with lithofacies 2 and 4.	Fluvial - sheetflood, possibly deltaic, and rare moderate energy lake shoreface	Uncommon. Sporadic in MOSZ at Gate and Buck. Also sporadic between 130 and 180 m, 220 and 280 m, and above 302 m at Gate, around 125 m and above 170 m in Buck, and around 170 m at Cowboy.
4. Tuff	Beds mostly massive and fine grained, 10 to 450 mm thick, interbedded with lithofacies 2 or 3, and rarely capping or grading from lithofacies 1. Coarser-grained tuffs can be a dark gray color whereas others have a light yellowish gray, dolomitic groundmass with occasional weathered (rusty) phenocrysts. Both types weather to a variably yellow to rusty-orange surface color.	Volcanic ash fall over any part of the lake. Tuffaceous sand/mud reworked into the lake by inflowing streams	Rare, but occur throughout the sections.

provided that such outcrop was within one meter of the required elevation (otherwise no "systematic" sample was taken). Additional supplementary samples were taken where visually distinct lithological variations were noted to occur that otherwise would have been missed by the 4 m sampling program. In particular, thin oil shale beds and some thin tuff beds were sampled, as was the more commonly interbedded MOSZ (figure 4).

The elemental compositions of the samples were analyzed by lithogeochemical methods at Actlabs, Canada, to a standard defined by ISO 17025. Analyses were undertaken in separate batches at different times: MOSZ samples from Buck and Gate locations separately, supra-MOSZ samples from Buck and Gate locations separately, and all the samples from the Cowboy location. This process can potentially introduce analytical differences into the data due to calibration variability in the analytical machine over time. However, this would be a normal complication expected whenever new wells are drilled and need to be correlated with an existing scheme. Results must be sufficiently robust to satisfy this situation.

In summary of the Actlabs procedures (from http://www.actlabs.com/), samples for elemental analyses are first crushed to a nominal minus 10 mesh (1.7 mm), mechanically split (riffle) to obtain a representative sample, and then pulverized using hardened steel (potentially contaminating with up to 0.2% Fe, 200 ppm Cr, and no more than trace amounts of Ni, Si, Mn, and C) to at least 95% passing the minus 150 mesh (106 microns). Resulting powders are mixed with a flux of lithium metaborate and lithium

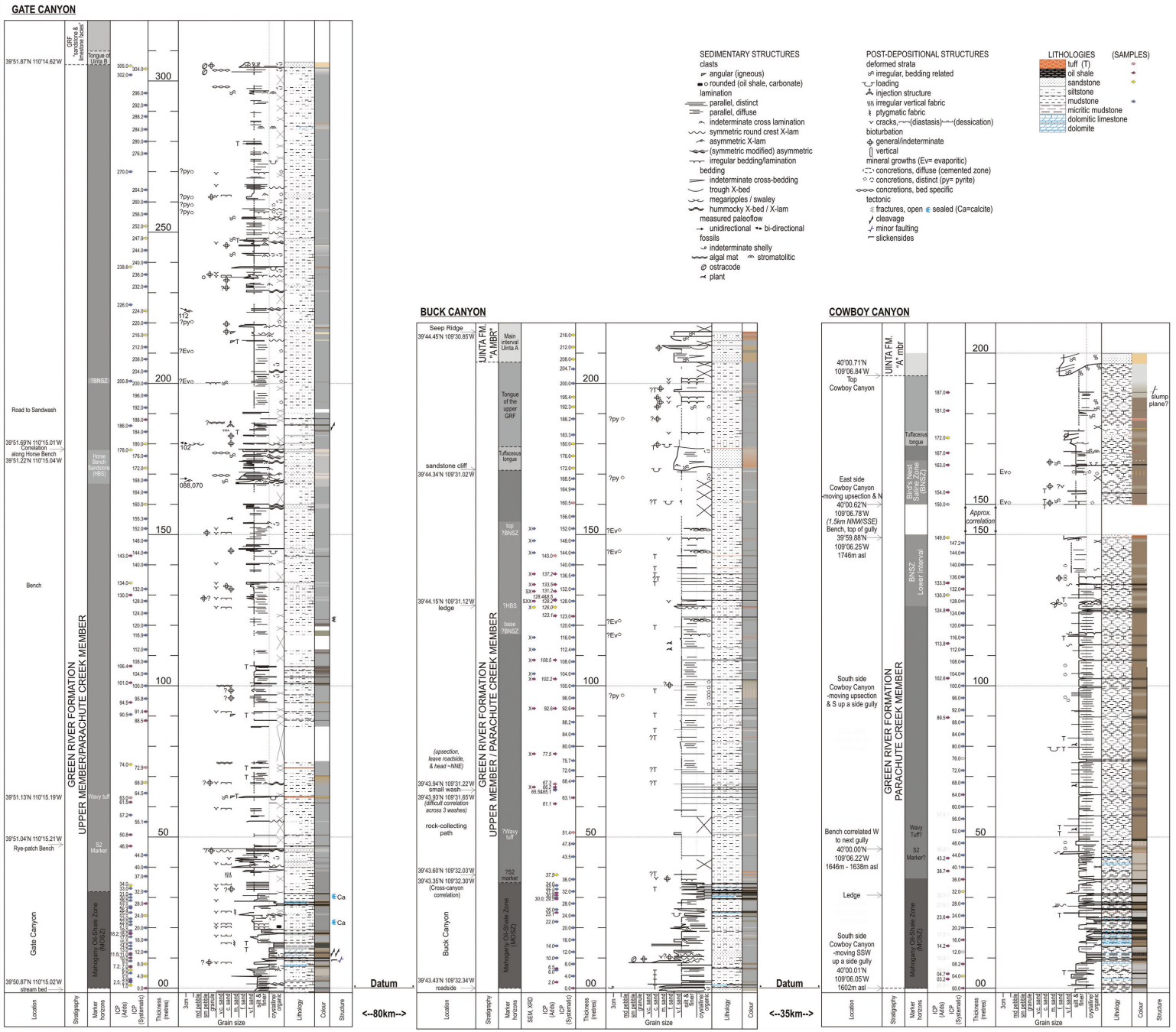

***Figure 4**. Summary sedimentary logs of outcropping upper Green River Formation strata at Buck, Gate, and Cowboy Canyons.*

tetraborate and fused in an induction furnace producing a melt that is mixed into a solution of 5% nitric acid until dissolved. Major oxide and selected trace-element content (table 2) are determined using a combination simultaneous/sequential Varian Vista ICP-OES (optical emission spectrometry), calibrated using seven prepared U.S. Geological Survey (USGS) and Canada Centre for Mineral and Energy Technology (CANMET) certified reference materials. The fraction, loss on ignition (LOI: organics and hydrated phases), for each sample is also calculated from these results. Sample material is then spiked with internal standards to cover the entire mass range, further diluted, and introduced into a Perkin Elmer SCIEX ELAN 6000, 6100, or 9000 ICP/MS using an Actlabs proprietary sample-introduction methodology to determine trace element abundance. The analytical lab describes this procedure as their "4 Litho" package, which results in a relative standard deviation from replicate analyses of <5% for major elements, and <10% for minor/trace elements, with uncertainties associated with the various determinations being + 15% at x 10 detection limit, and + 5% at x 100 detection limit. This preparation method is noted by Actlabs to be less accurate for recording the abundance of base metals (Cu, Pb, Zn, and Ni), plus As, Bs, W (at >100 ppm), Sn (at >50 ppm) and Cr (at >1,000 ppm). Since these elements were not expected to play a major role in the chemostratigraphic study (but see below), uniformity of sample preparation was preferred for the current study.

The basic results are presented in tabular form in appendix I and presented graphically in subsequent appendices for each logged section in turn (appendices II to IV). "Height" (vertical thickness above base MOSZ) versus abundance (wt %) plots are provided for each of the major oxides (SiO_2, Al_2O_3, Fe_2O_3(T), MnO, MgO, CaO, Na_2O, K_2O, TiO_2, and P_2O_5). Similar plots are also included for many of the trace elements analyzed, measured in parts per million (ppm): Sc, V, Cr, Co, Cu, Zn, Ga, As, Rb, Sr, Y, Zr, Nb, Mo, Sn, Sb, Cs, Ba, La, Ce, Pr, Nd, Sm, Eu, Gd, Tb, Dy, Ho, Er, Tm, Yb, Lu, Hf, Ta, W, Tl, Pb, Bi, Th, U. Although ICP allows for the recognition of ppm abundances of trace elements, in numerous cases (see table 2) the Actlabs reading is below their detection limits. Where this is the case for an element, subsequent statistical analysis is inappropriate (non-parametric statistics are possible where only one reading is below the detection limit). For elements such as Be, Ge, Ag, Ni, and In, which record abundances mostly below detection limits, no depth plots have been produced.

The raw data are also manipulated to indicate abundances relative to an external standard, specifically as a ratio of the abundance of a particular element to that element's abundance in Post-Archean Average Shale (PAAS)—comparison is also made with the USGS standard shale from the MOSZ of the GRF in the Piceance Creek Basin: sample SGR-1. These ratio data are plotted as a spider diagram for each sample (appendices V to VII). In addition, the data also have been transformed to counter the "constant sum problem" that is inherent in compositional data (i.e., data expressed as % or ppm) and that results in forced correlations (see review in Pawlowsky-Glahn and Egozcue, 2006). The resulting centered log-ratio values are not reproduced in their entirety since it is stressed that *any* statistical treatment undertaken of the data must be considered only a guide to potential trends, simply due to the previously noted field-sampling constraints: ratios, plotted against depth, are reproduced only for selected data in subsequent figures. Finally, ratios for different pairs of elements, with known mineralogical associations, are plotted against height above base MOSZ (plots are again reproduced only for selected data in subsequent figures).

The presence of certain anomalous values in the whole-rock ICP data for this project raised questions as to the associated mineral phase, both the actual mineral present and its detrital or diagenetic origin. To this end some additional sample material has been processed for XRD and SEM analyses. In such analyses, results are ascertained by a Bruker AXS D8 solid state powder diffraction XRD system using additional, similarly prepared, powdered samples, and by a Hitachi SU 70 FEG-SEM with attached Oxford Instruments INCA solid-state EDS using remaining sample chips (both at the University of New Brunswick). For the XRD analysis, powder is compacted into the circular well of a plastic sample holder and placed on the sample stage with three reference points for sample height. The X-ray source is a sealed, 2.2 kW Cu X-ray tube, maintained at an operating current of 40 kV and 30 mA, and the X-ray optics comprise a divergence slit (1.00 mm), anti-scatter receiving slit (1.00 mm) and detector slit (0.20 mm). Samples have been scanned in the range of 5 to 90° (2θ) using a step size of 0.02° and a step time of 1.0 sec. Detection is via a Peltier-cooled solid-state [Si(Li)] detector (Sol-X) with a useful energy range of 1 to 60 KeV; a set of 2° Soller slits are used in order to lower horizontal beam divergence, and no correction is made for Kβ radiation. Phase identification is made with a combination of the Windows-based programs Bruker Eva and MDI Jade; the reference-intensity-ratio method is used to estimate the weight fractions of the different phases.

Remaining chips from three samples of interest from Buck Canyon have been split in half for optical microscopy and SEM. One half has been further cut and polished as a standard thin section along a cross-sectional surface. The other half has been cut, polished and carbon coated along the counterface cross-section and on a bedding surface. Optical microscopy uses a Nikon E400 polarizing microscope with E5400 digital camera, and scanning electron microscopy employs a Hitachi SU 70 FEG-SEM with attached Oxford Instruments INCA solid-state EDS (also at UNB). The sample from the 152 m in Buck Canyon required additional heating to 100°C to eliminate problems in the vacuum chamber caused by degassing. Initial mapping of con-

***Table 2**. List of elements analyzed by ICP methods.*

Element (atomic number)	Classifications			Analysis Method	Analyte Symbol	Units	Detection Limit	# of samples with values below detection		
	Abundance	Catergory	Other					Gate	Buck	Cowboy
Sodium, Na (11)	major	alkali metal		FUS-ICP	Na2O	%	0.01	0	0	0
Magnesium,Mg (12)	major	alkali earth metal		FUS-ICP	MgO	%	0.01	0	0	0
Aluminum, Al (13)	major	post-transition metal		FUS-ICP	Al2O3	%	0.01	0	0	0
Silicon, Si (14)	major	metalloid		FUS-ICP	SiO2	%	0.01	0	0	0
Phosphorus, P (15)	major	non-metal		FUS-ICP	P2O5	%	0.01	0	0	0
Potassium, K (19)	major	alkali metal		FUS-ICP	K2O	%	0.01	0	0	0
Calcium, Ca (20)	major	alkali earth metal		FUS-ICP	CaO	%	0.01	0	0	0
Titanium, Ti (22)	major	transition metal		FUS-ICP	TiO2	%	0.001	0	0	0
Manganese, Mn (25)	major	transition metal	base metal	FUS-ICP	MnO	%	0.001	0	0	0
Iron, Fe (26)	major	transition metal	(base metal)	FUS-ICP	Fe2O3(T)	%	0.01	0	0	0
Beryllium, Be (4)	trace	alkali earth metal		FUS-ICP	Be	ppm	1	>1	>1	>1
Scandium, Sc (21)	trace	transition metal	(REE)	FUS-ICP	Sc	ppm	1	0	1	0
Vanadium, V (23)	trace	transition metal		FUS-ICP	V	ppm	5	0	0	0
Chromium Cr (24)	trace	transition metal		FUS-MS	Cr	ppm	20	>1	>1	>1
Cobalt, Co (27)	trace	transition metal		FUS-MS	Co	ppm	1	>1	0	>1
Nickel, Ni (28)	trace	transition metal	base metal	FUS-MS	Ni	ppm	20	>1	>1	>1
Copper, Cu (29)	trace	transition metal	base metal	FUS-MS	Cu	ppm	10	>1	>1	>1
Zinc, Zn (30)	trace	(post-)transition metal	base metal	FUS-MS	Zn	ppm	30	>1	>1	>1
Gallium, Ga (31)	trace	post-transition metal		FUS-MS	Ga	ppm	1	>1	0	0
Germanium, Ge (32)	trace	metalloid		FUS-MS	Ge	ppm	1	>1	>1	>1
Arsenic, As (33)	trace	metalloid		FUS-MS	As	ppm	5	>1	>1	>1
Rubidium, Rb (37)	trace	alkali metal		FUS-MS	Rb	ppm	2	0	0	0
Strontium, Sr (38)	trace	alakli-earth metal		FUS-ICP	Sr	ppm	2	0	0	0
Yttrium, Y (39)	trace	transition metal	REE (heavy)	FUS-ICP	Y	ppm	2	0	0	0
Zirconium, Zr (40)	trace	transition metal		FUS-ICP	Zr	ppm	4	0	0	0
Niobium, Nb (41)	trace	transition metal	refractory metal	FUS-MS	Nb	ppm	1	>1	0	1
Molybdenum, Mo (42)	trace	transition metal	refractory metal	FUS-MS	Mo	ppm	2	>1	>1	>1
Silver, Ag (47)	trace	transition metal	precious metal	FUS-MS	Ag	ppm	0.5	>1	>1	>1
Indium, In (49)	trace	post-transition metal		FUS-MS	In	ppm	0.2	>1	>1	>1
Tin, Sn (50)	trace	post-transition metal		FUS-MS	Sn	ppm	1	>1	>1	>1
Antimony, Sb (51)	trace	metalloid		FUS-MS	Sb	ppm	0.5	>1	>1	>1
Cesium, Cs (55)	trace	alkali metal		FUS-MS	Cs	ppm	0.5	>1	0	1
Barium, Ba (56)	trace	alakli-earth metal		FUS-ICP	Ba	ppm	3	0	0	0
Lanthanum, La (57)	trace	lanthanoid	lightREE	FUS-MS	La	ppm	0.1	0	0	0
Cerium, Ce (58)	trace	lanthanoid	lightREE	FUS-MS	Ce	ppm	0.1	0	0	0
Praseodymium, Pr (59)	trace	lanthanoid	lightREE	FUS-MS	Pr	ppm	0.05	0	0	0
Neodymium, Nd (60)	trace	lanthanoid	lightREE	FUS-MS	Nd	ppm	0.1	0	0	0
Samarium, Sm (62)	trace	lanthanoid	middleREE(light)	FUS-MS	Sm	ppm	0.1	0	0	0
Europium, Eu (63)	trace	lanthanoid	middleREE(light)	FUS-MS	Eu	ppm	0.05	0	0	0
Gadolinium, Gd (64)	trace	lanthanoid	middleREE(heavy)	FUS-MS	Gd	ppm	0.1	0	0	0
Terbium, Tb (65)	trace	lanthanoid	middleREE(heavy)	FUS-MS	Tb	ppm	0.1	>1	1	0
Dysprosium, Dy (66)	trace	lanthanoid	middleREE(heavy)	FUS-MS	Dy	ppm	0.1	0	0	0
Holmium, Ho (67)	trace	lanthanoid	middleREE(heavy)	FUS-MS	Ho	ppm	0.1	1	1	0
Erbium, Er (68)	trace	lanthanoid	heavyREE	FUS-MS	Er	ppm	0.1	0	0	0
Thulium, Tm (69)	trace	lanthanoid	heavyREE	FUS-MS	Tm	ppm	0.05	1	0	0
Ytterbium, Yb (70)	trace	lanthanoid	heavyREE	FUS-MS	Yb	ppm	0.1	0	0	0
Lutetium, Lu (71)	trace	lanthanoid	heavyREE	FUS-MS	Lu	ppm	0.04	0	0	0
Hafnium, Hf (72)	trace	transition metal		FUS-MS	Hf	ppm	0.2	0	0	1
Tantalum, Ta (73)	trace	transition metal	refractory metal	FUS-MS	Ta	ppm	0.1	>1	0	>1
Tungsten, W (74)	trace	transition metal	refractory metal	FUS-MS	W	ppm	1	>1	>1	>1
Thallium, Tl (81)	trace	post-transition metal		FUS-MS	Tl	ppm	0.1	>1	0	>1
Lead, Pb (82)	trace	post-transition metal	base metal	FUS-MS	Pb	ppm	5	>1	>1	>1
Bismuth, Bi (83)	trace	post-transition metal		FUS-MS	Bi	ppm	0.4	>1	>1	>1
Thorium, Th (90)	trace	actinoid		FUS-MS	Th	ppm	0.1	0	0	0
Uranium, U (92)	trace	actinoid		FUS-MS	U	ppm	0.1	0	0	0

tiguous/adjoining ~300 µm by ~400 µm areas from top to bottom of each cross-sectional sample uses the INCA mapping tool with 5 minute acquisition times (~2 million counts), complemented with a BSE image of the same area. Selected INCA elemental maps are then color coded and, using Corel software, overlain on the BSE image before being cropped, and montaged to help identify mineral phases. Areas or mineral associations of greater interest are then mapped at greater resolution or spot analyzed for elemental composition.

SEDIMENTOLOGICAL LOGS

Gate Canyon

The MOSZ and upper GRF succession commences near the top of Gate Canyon and extends northward, past the turnoff for Sand Wash, toward the watershed between Nine Mile Canyon and Wells Draw (figure 2B). Most recently, Remy (1992) measured part of this succession at roughly the same location in Gate Canyon and calculated a thickness of ~36 m from base MOSZ up to his S2 marker, and a further 111 m to base HBS. Unfortunately, the log for his "section 19" was not included in his work. It can therefore be speculated that his base MOSZ equates to the oil shale at 10 m in this report because, herein, the S2 marker is identified at ~46 m, and the base HBS can potentially be extended down to a sandstone at ~158 m (although herein the base HBS is considered higher in the section at ~166 m).

For this study, the succession was measured in three component subsections (figure 2). The MOSZ was measured on a west-facing slope at the top of Gate Canyon where thin (very-) fine-grained sandstone beds and a lens of intraclastic pebbly sandstone interbed with variably calcareous mudstone and organic-rich, often papery shale (figure 4). At several horizons, deposition can be considered to have been under shallow or marginal lacustrine conditions: some sandstone contains wave-modified current ripples, and some mudstone shows evidence both of cracks that may be interpreted as both diastasis and desiccation in origin, and a fabric that is reminiscent of a blocky ped (i.e., paleosol). Stray large boulders of oil shale are encased in gray shale, indicating reworking of precursor oil shale beds, likely during one of the lake low-stands that formed some of the aforementioned shallow-water features.

At approximately the level of Remy's S2 marker, a resistant bed which helps form Rye Patch Bench, the strata were traced laterally northwest back to the Gate Canyon road, where measurement of the vertical section resumed. Exposure immediately above Rye Patch Bench is poor throughout the area and even estimations of vertical thickness are difficult across the shallow-gradient slopes: only resistant tuff (including Wavy tuff at 63 m), sandstone, and oil shale typically outcrop. As sandstone beds become thicker and more common upsection, the exposure improves, culminating at the top of the major ledge-forming HBS (178 m). In Gate Canyon, the HBS corresponds to several grossly coarsening upward (rarely fining upward) sandstone packages that display numerous features interpretive of a lacustrine shoreface, including hummocks, wave ripples, current ripples (often with wave-modified tops), and diastasis (or synaeresis) cracks.

The top of the HBS was used to correlate the succession further to the northwest to where the Gate Canyon Road meets the Sand Wash Road; the latter runs along the top of HBS for several miles to the east. The third measured subsection extends north from this junction. Within the lowermost slope was the highest exposed oil shale (188 m) at this location and a slightly olive green colored horizon (200.8 m) with displacive and lamina-disruptive calcite nodules up to 5 mm diameter, which is tentatively considered a possible westward extension of the BNSZ. Although containing many of the same structures as previously mentioned, sandstone beds are usually isolated, rather than forming packages, and become less common upsection. Above an interval with abundant rusty nodules (probably weathered pyrite, between 260 and 270 m), occasional beds of algal mats and stromatolites are present (e.g., 284 m).

The top of the measured section in this report corresponds to a ledge-forming sandstone at 304 m that contains numerous ostracodes and that is bioturbated and widely internally deformed (soft sediment). Above this bed, thick cross-stratified sandstone beds, interpreted as fluvial in origin, become more common and distinct; white-weathering, chalky micrite beds are also found. On recent geologic maps, the sandstone ledge has been marked as the boundary between the upper GRF and the GRF "sandstone and limestone facies," with the "saline facies" having pinched out approximately at this boundary ~17.5 km to the west of Gate Canyon (Weiss and others, 1990; Witkind, 1995). However, the lithofacies at 304 m and immediately above are also typical of a Uinta Formation, B member, interbedded sandstone and mudstone, and can alternatively be considered a basal interfingering of that formation.

Buck Canyon

The entire upper GRF succession has been examined at Buck Canyon, which is a side canyon of Willow Creek Canyon (figure 2C). To this author's knowledge, the succession has not previously been measured at this location, although Cashion (1967, his section H) measured the same interval in Willow Creek Canyon, ~5 km west of the current study area. In this earlier work, the HBS was measured ~122 m above base MOSZ, but the base Uinta Formation was not taken at the sandstone beds forming Seep Ridge, but significantly higher up in the succession,

closer to where Sprinkel (2008) maps the base of the Uinta Formation B member.

For this study, the measurements are again from a composite of three subsections measured at different points along Buck Canyon (figure 2C). The MOSZ was measured on a northwest-facing slope close to half-way up Buck Canyon (figure 2C), where it attains a thickness of ~35 m (figure 4). Several <20 cm-thick beds of calcareous sandstone (pebbly or ostracode-rich coarse-grained sandstone and finer grained, coarsening- and fining-upward, bioturbated and non-polygonal-cracked symmetric and asymmetric rippled sandstone) irregularly interbed with variably shaley and organic-rich, gray and greenish gray, marly mudstone. Thin interbeds of oil shale are often papery, and are thickest and most common near the top of the MOSZ where the oil shale appears deformed by syn-sedimentary folding and faulting.

The MOSZ is capped by a couple of bench-forming, orange-weathering, marly, very fine grained tuffaceous sandstone beds that can be traced northward and correlated across the Buck Canyon road and may correspond to Remy's S2 marker in Gate Canyon. Above these beds, the succeeding 20 to 25 m of section is difficult to accurately measure, being very poorly exposed on very gentle, soil-covered slopes, but appears dominated by gray mudstone with only isolated thin ledges of outcropping tuffaceous sandstone (possibly including the Wavy tuff at 51.4 m) and oil shale.

A series of 5 to 20 cm-thick oil shale beds, typically spaced 0.5 to 2 m apart, mark the start of the better exposed section further up the canyon (~60 m upward). They persist, along with thin tuffs, within a thick succession of gray and light gray, rarely beige to olive to mottled orange carbonate mudstone. The mottling is associated with rusty-weathering nodules, assumed after pyrite alteration, and lenticular-cracked (interpreted as due to synaeresis or diastasis) siltstone. Laminae are further disrupted by extensive mm-scale, angular crystal aggregates of calcite at 120 m, a horizon herein considered equivalent to the base of the BNSZ farther east.

At 126 m above the base of the MOSZ is a ~0.7 m-thick ledge of orange-weathering, light gray, rippled, coarsening-upward silty to very fine grained, and slightly tuffaceous calcareous sandstone. This bed appears to have been correlated with the HBS by Sprinkel (2008), a correlation followed in this report. The uppermost oil shale in Buck Canyon is recorded at ~137 m, at a similar height in the section as the uppermost oil shale assayed by Cashion (1967). Thin tuff beds, some distinctly jointed, continue to interbed upsection. Additional rusty-nodular intervals are also present along with, at 144 and 152 m, two zones of slightly olive-green weathering marly mudstone where the lamination is again disrupted by large angular calcite and dolomite crystals. Correlation with the outcropping "bird's-nest zone" (upper BNSZ) is suggested, since both zones occur at a stratigraphically similar level, ~25 m below the first distinctively tuffaceous sandstone at each location.

At 171 m above base MOSZ is a ledge-forming, distinctly orange-weathering, non-calcareous, beige-coloured, variably tuffaceous sandstone dominated by convolute laminations and massive beds above its extensively loaded basal contact. This bed is mapped by Sprinkel (2008) as the base of the Uinta Formation, interfingering and pinching out westward into upper GRF mudstone. On the north side of Buck Canyon it is overlain by gray siltstone, gray-green marly mudstone, and whitish gray, silty mudstone that in turn are capped by two stacked sandbodies (~207 to 216 m). These sandstone beds form Seep Ridge and are characterized by beige-orange, variably (non-) calcareous, fine- to medium-coarse-grained sandstone containing cross-stratification, asymmetrical laminations, and convolutions. These beds are considered the base of the main body of the Uinta Formation "A member", as similarly mapped by Sprinkel (2008).

Cowboy Canyon

The entire upper GRF succession has been examined at Cowboy Canyon, which is a side canyon of White River Canyon (figure 2D). Again, the succession at Cowboy Canyon has not previously been measured, but Cashion (1967, his section M) measured the same interval in Evacuation Creek Canyon, ~6 km south of the current study area. In this earlier work, the base of the Uinta Formation was measured ~140 m above base MOSZ, and the base of the "Evacuation Creek Member" (equated to the HBS) was measured ~90 m above base MOSZ. As noted below, this would be inconsistent with his mapped contacts at Cowboy Canyon.

The entire upper GRF succession has been examined from a composite of two subsections measured at different points along Cowboy Canyon (figure 2D). Much of the succession is exposed in gullies and on the promontory at the southeast end of Cowboy Canyon. On the northeast-facing slope, the MOSZ is predominantly variable brown to black carbonate-rich shale with variably thick oil shale beds forming a series of steep narrow ledges. Locally the oil shale is papery and internally deformed and faulted. Although thin tuffaceous beds are present, sandstone is restricted to a thin, fining-upward sandstone near the top of the MOSZ (32 m) and a thin, channelized, lenticular sandstone (~45 m) just above it. Sandstone is similarly rare in the overlying interval, which is again dominated by variably organic-rich carbonate shale. A few thin oil shale and tuff beds are indistinctly exposed. Most notable are large decimeter-scale radial casts of dissolved saline crystalline aggregates at ~128 m. The section on the promontory

is capped by orange-brown beds of tuffaceous siltstone (~147 m) that are loaded down into underlying siltstone. Both Cashion (1967) and Sprinkel (2008) map the cap as equivalent to the HBS.

This tuffaceous siltstone forms a variably wide bench to the north of the White River Canyon, allowing for an approximate correlation to similar rusty beds at the head of Cowboy Canyon. Overlying is an interval with numerous dissolution cavities and locally nodular calcite-gypsum aggregates: the BNSZ. On top of this are variable internally contorted shale, thin oil shale beds, and a tuffaceous silty sandstone. Just below the highly deformed and loaded contact with the Uinta Formation, another oil shale appears to be in a faulted repeat section.

Potential Correlations

As noted in the descriptions above, there remains doubt as to the correlation of beds within the measured sections. Following a more layer-cake stratigraphy, the tuffaceous sandstone bed(s) at Buck and Cowboy Canyon might be considered the lateral equivalent of the HBS (figure 5A, 5B), with the unit pinching out northward just to the northwest of Buck Canyon (figure 2C). This requires a lateral facies change in the composition of the HBS over the ~80 km west to Gate Canyon: from tuffaceous, locally trough cross-bedded, often loaded or soft-sediment deformed, medium- to fine-grained sandstone in the east to much less tuffaceous, wave-rippled, finer grained, occasionally coarsening-upward sandstone in the west. More problematic, is that this scheme puts the BNSZ in Cowboy and Buck below the HBS, while this study identifies strata more akin to the BNSZ sitting above the HBS in Gate (note Cashion, 1967, considered the HBS at Cowboy equivalent to the tuffaceous sandstone at ~150 m, which would put the BNSZ above the HBS; the overlying tuffaceous sandstone would then have to pinch out westward between Cowboy and Buck).

The sandstone at 126 m in Buck Canyon, alternatively, may be correlated with one of the sandstone beds between 130 m and 180 m in Gate Canyon (essentially the HBS succession). Two scenarios are put forward for the HBS correlation. Since the sandstone in Buck Canyon coarsens upward, a tie-in with a similarly profiled sandstone at ~135 m in Gate Canyon might make sense (figure 5C). This would mean that the main ledge-forming HBS sandstone must pinch out eastward, with this and the underlying sandstone beds forming part of a retrogradational parasequence set, and the interval where there is a significant thickening of the section. If the 126 m sandstone at Buck is alternatively correlated with one of the higher HBS sandstone beds in Gate Canyon (figure 5D), the interval of significant section thickening would be lower in the succession. Both options allow for the uppermost ("last") oil shale beds in Buck and Gate, and the top of the BNSZ to roughly parallel the HBS, with the tuffaceous sandstone in Buck and Cowboy Canyons simply pinching out to the west of Buck Canyon (figure 2C).

ICP RESULTS SUMMARY

Review of Previously Analyzed Data from Buck Canyon

The preliminary samples from the upper GRF at Buck Canyon, collected as part of a previously unpublished UGS-supported study (that also analyzed samples from the lowermost strata of the Uinta Formation), included sandstone (n = 6 samples), tuff (n = 5), mudstone (n = 38), and oil shale (n = 2). This preliminary work identified several possible patterns in the data, including elevated values for particular elements in different samples (peak anomalies), elements whose abundance appeared directly related to the lithofacies type, and elements, or ratios of elements, whose values increased or decreased sharply or gradually with measured height in the section.

Several samples exhibited peak anomalies in many of the rare earth elements (REEs), plus Sr, U, Th, and P. The latter (as P_2O_5, in wt %, as determined from fusion-ICP, see table 2) was particularly notable, with a mean value (μ) of 0.211 wt % for the 51 samples, but including two anomalous samples, one being a gray shale with P = 0.63 wt %, and the other being an oil shale (lying slightly below the uppermost recorded oil shale) with P = 6.22 wt %. The phosphatic oil shale was also one of four samples with anomalously high values of the heaviest REEs; PAAS-normalized spider diagrams further indicated that the enrichment occurs gradually but consistently from lightest to heaviest REE in the phosphatic oil shale (figure 6). The other samples with anomalous heavy-REE values were a tuff (~104 m) and adjacent gray- and olive-colored silty shale beds at ~119.0 and 119.5 m. In contrast, the olive-colored silty shale at ~68 m showed anomalous enrichment only in lighter REEs.

New ICP Data: Gate, Buck, and Cowboy Canyons

Data Collection Summary

In the subsequent discussion, all samples are uniquely named by a prefix denoting to which of the three datasets they belong (GC = Gate Canyon, BC = Buck Canyon, CC = Cowboy Canyon), and the height in meters above base MOSZ from which they were taken within each section (for example, GC002 refers to a sample collected 2 m above base MOSZ in Gate Canyon).

Systematic sampling at 4 m vertical stratigraphic spacing

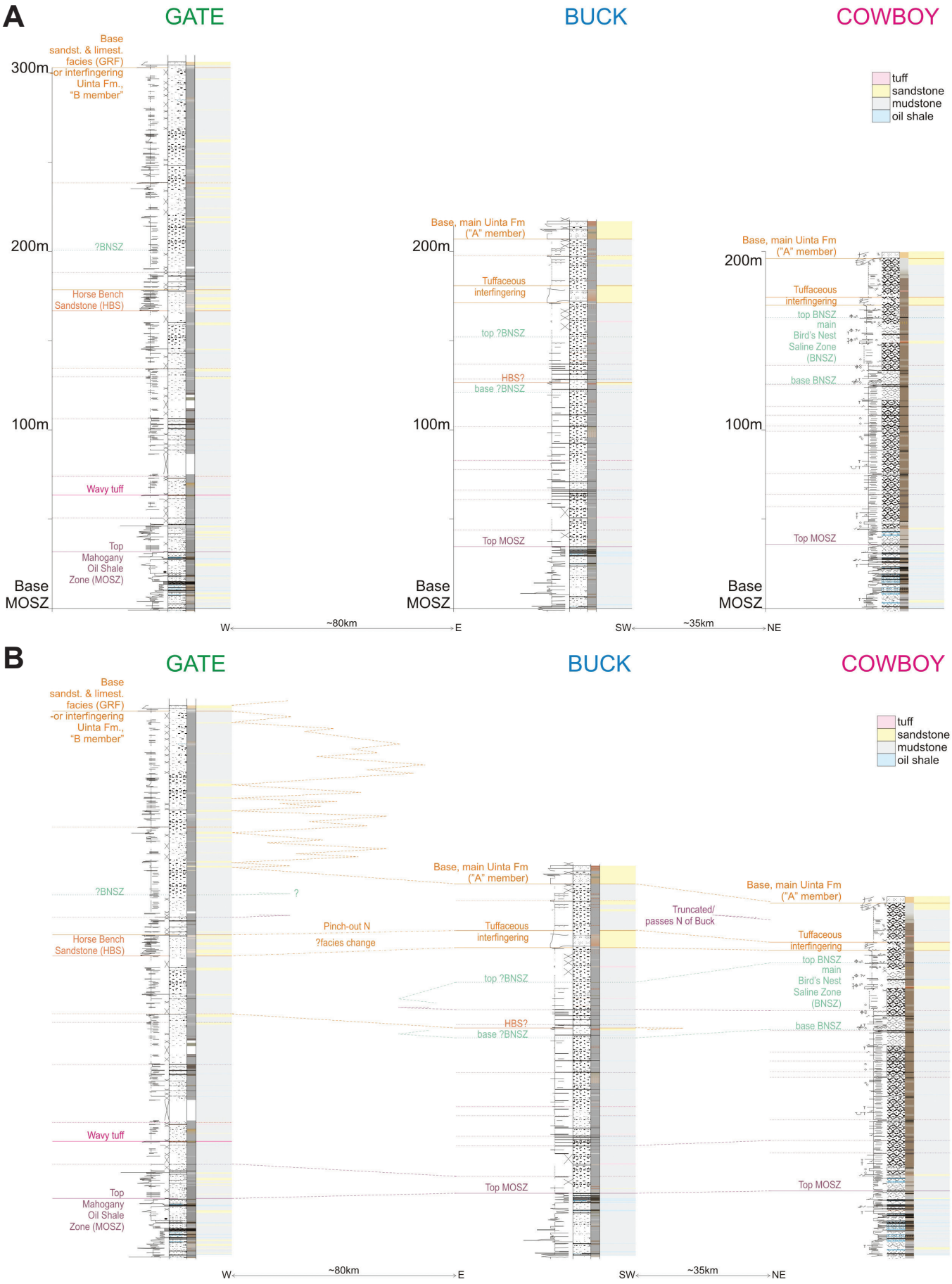

Figure 5*. Potential correlations of strata at Buck, Gate, and Cowboy Canyons. (A) Beds identified at the three canyons and their stratigraphic elevation. (B), (C), and (D) represent three potential correlations, the applicability of each is discussed in the text.*

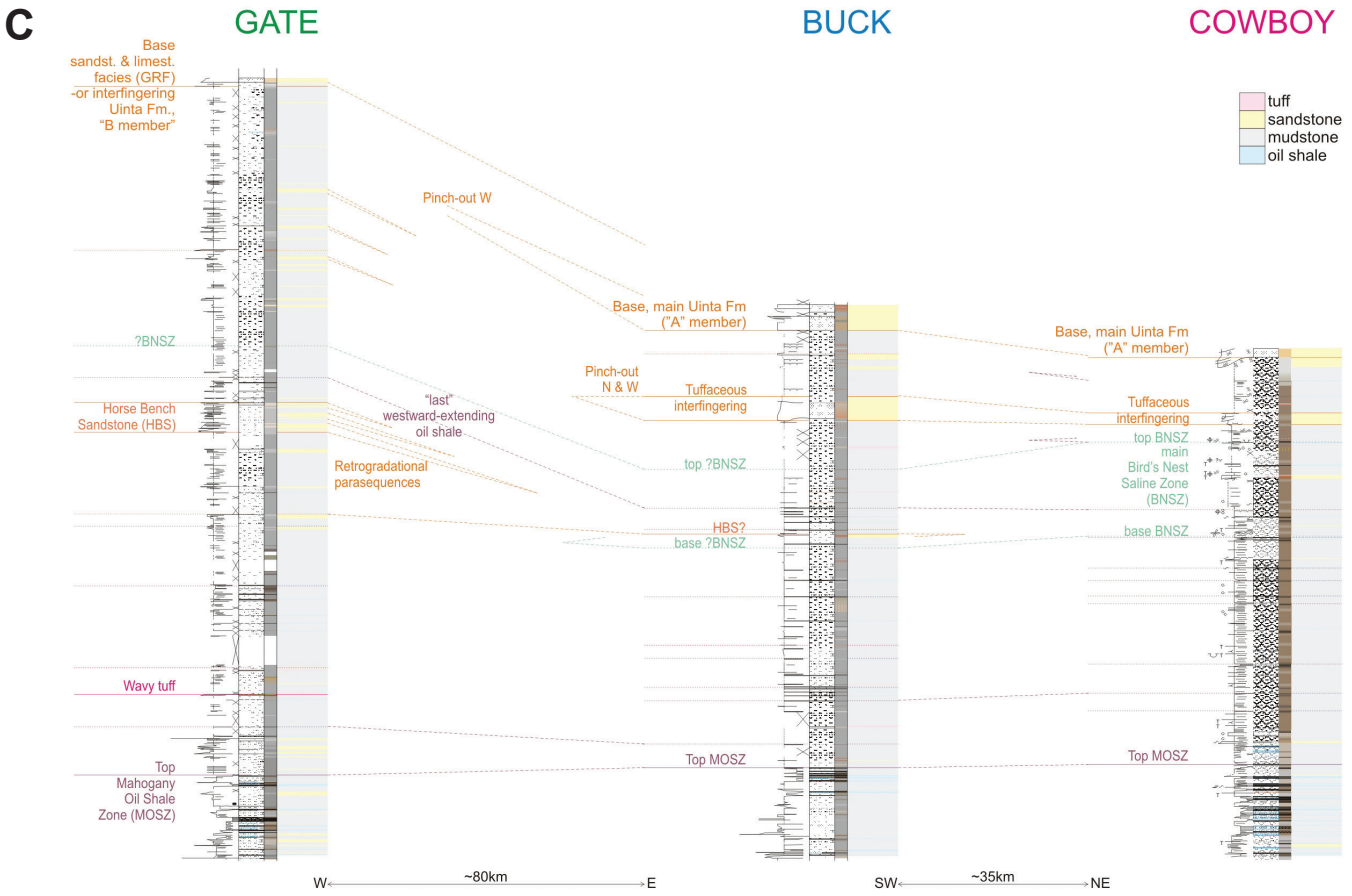

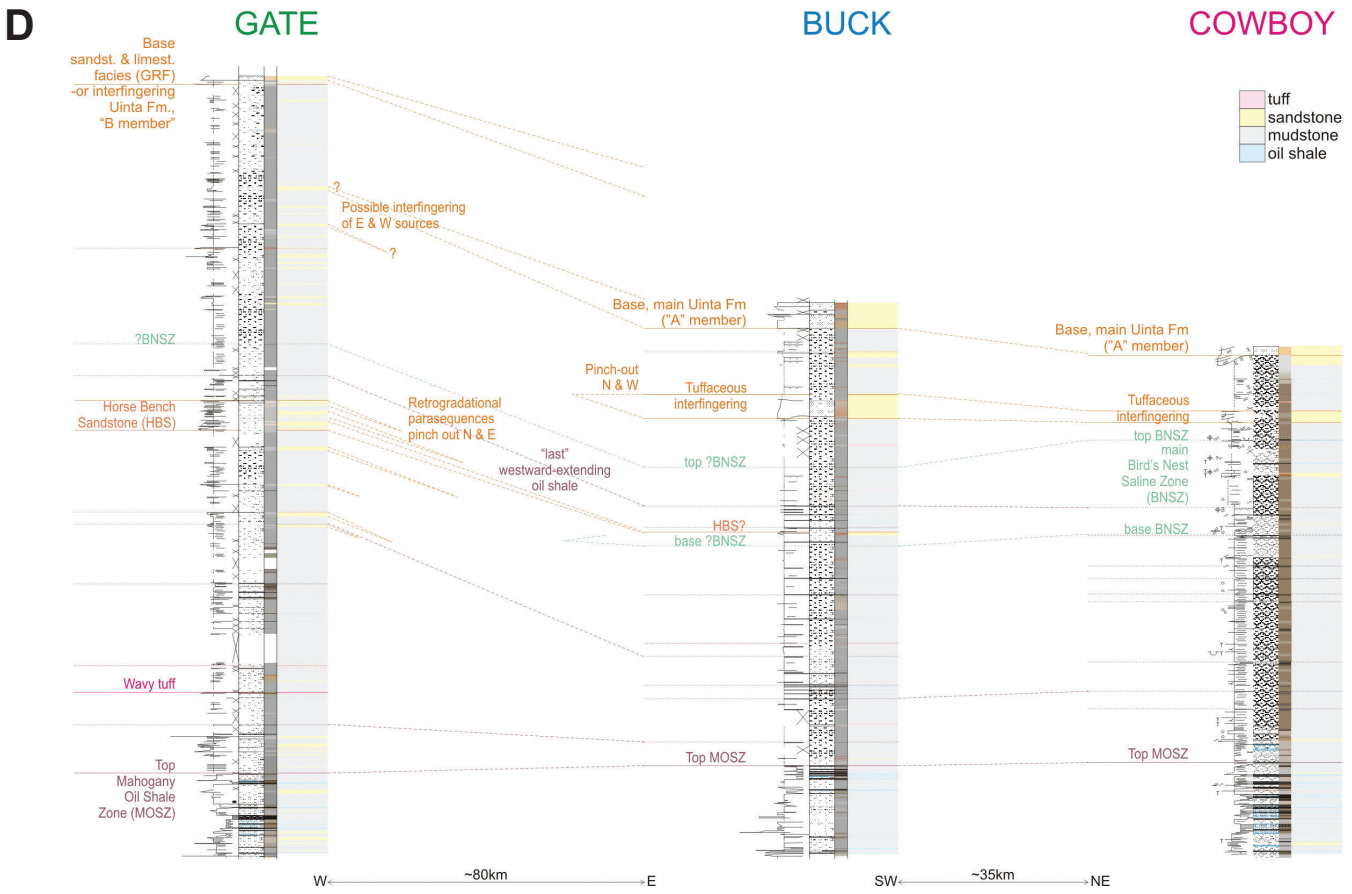

***Figure 5**. Continued.*

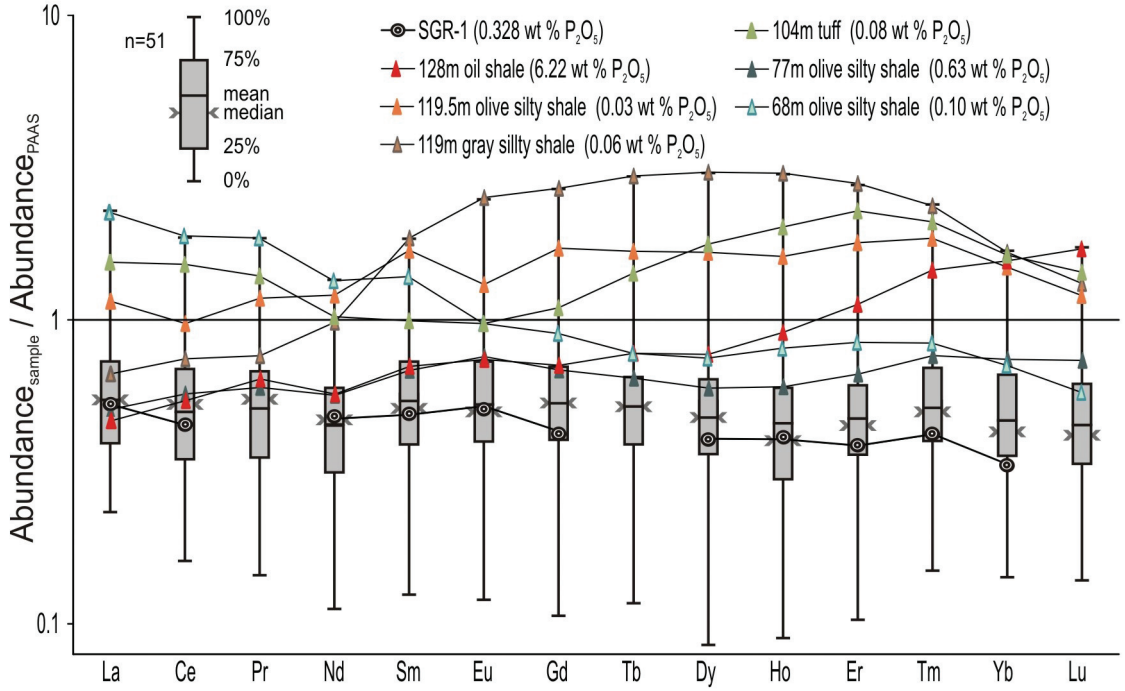

***Figure 6**. Summary statistics of the rare earth elements taken from selected previous analyses at Buck Canyon (UGS unpublished data) and expressed as box-whisker spider plots of abundance against Post-Archean Average Australian Shale (PAAS; Taylor and McLennan, 1985; McLennan, 1989). Equivalent values for the USGS reference material SGR-1 (USGS website, 2010) are included for comparison.*

along Gate Canyon collected a total of 66 samples for analysis, comprising mudstone (n = 48), sandstone (n = 12), tuff (n = 1), and oil shale (n = 5). An additional 51 samples were taken from the measured section at beds of particular interest, comprising an additional 28 mudstone, 8 sandstone, 1 tuff, and 14 oil shale samples, giving a total of 117 samples analyzed from this section (figure 4 and appendix Ia). The Gate Canyon samples were analyzed in two batches, one containing samples from the MOSZ, the other samples from above the MOSZ, plus four additional MOSZ samples.

The 4 m systematic sampling along Buck Canyon—taken close to the section from where the preliminary dataset was recovered—collected mudstone (n = 37), sandstone (n = 7), tuff (n = 3), and oil shale (n = 5) for a total of 52 samples. An additional 11 mudstone, 1 sandstone, 1 tuff, and 24 oil shale samples were collected from beds of particular interest, resulting in 37 supplementary samples, and a combined total of 89 samples from this section (figure 4 and appendix Ib). The Buck Canyon samples were analyzed in two batches, one containing samples from above the MOSZ, the second samples from the MOSZ, plus replicates from two beds higher up in the section found to be of interest.

At Cowboy Canyon, the 4 m sampling interval resulted in the collection of material from 30 mudstone and 6 oil shale beds (total: n = 36) from the succession measured on the promontory. Supplementary sampling of additional oil shale beds (n = 16), mudstone (n = 2), and tuffaceous sandstone (n = 2) from both the promontory and the upper measured section, resulted in an additional 20 samples for a combined total of 56 samples (figure 4 and appendix Ic).

Anomalous Elemental Peaks: Phosphorus

Phosphorus values in the three sections average well under 1.0 wt % (Gate mean, μ = 0.19, median (M) = 0.07; Buck, μ = 0.72, M = 0.08; Cowboy, μ = 0.5, M = 0.09). Mean values are higher due to several samples in each canyon being highly enriched in P, with the anomalies confirmed when the data are normalized against Si (figure 7A). The enrichment is most pronounced in examples from the more easterly, basinward sections.

Samples containing over 1.5 wt % phosphorus at Gate Canyon are exclusively oil shale, specifically, GC18, GC50.8, GC91.4, and GC130, with GC31, a micritic shale, also having a value over 1.0 wt % (appendix II). In Buck Canyon (appendix III), two replicates were taken from each of two oil shale beds, BC77.5 and BC128.2. In the lower bed, values were 9.01 and 9.47 wt %. In a few schemes (reviewed by Slansky, 1986) the rock is very close to being classified as a phosphorite deposit. The upper bed returned values of over 6 % (6.04 and 6.29 wt %) but, notably, the base of the same oil shale (BC128.1) records a value of 0.06 wt %, and samples of overlying mudstone (BC128.4 and BC128.5) both have values of 0.08 wt %. This phosphatic horizon, therefore, is highly localized stratigraphically,

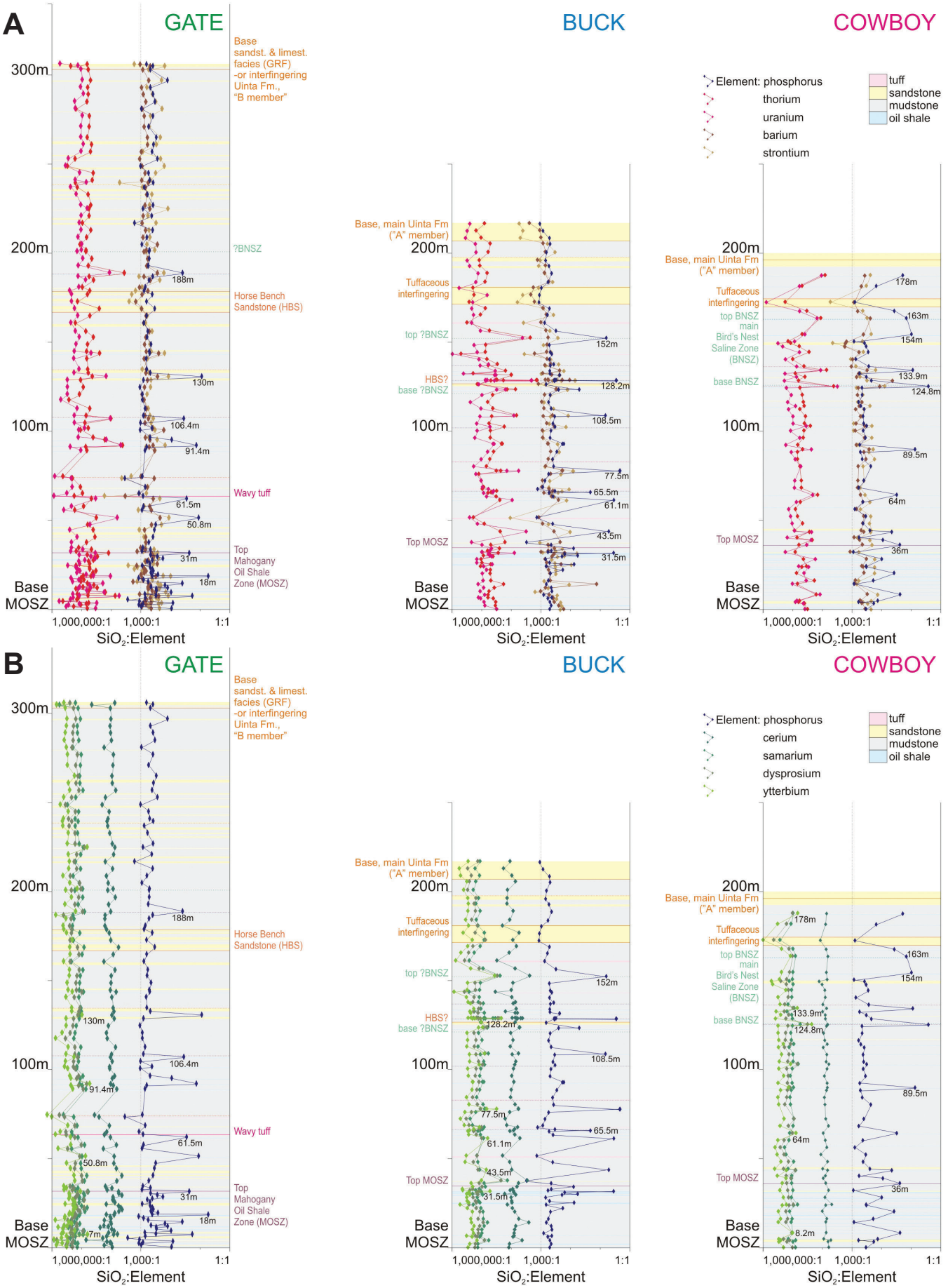

***Figure** 7. Ratio-elevation plots for silicon against selected elements at Buck, Gate, and Cowboy Canyons. (A) phosphorus, uranium, thorium, barium, and strontium, (B) phosphorus, cerium, samarium, dysprosium, and ytterbium.*

being confined to the upper 10 cm of the oil shale bed. Other phosphatic oil shale beds at Buck Canyon (P >1.0 wt %) are identified in BC31.5, BC43.5, BC61.1, BC65.5, and BC108.5. One other sample records an anomalously high P content: BC152 m, an olive-gray evaporitic mudstone with chemically disrupted bedding and large diagenetic crystals, contains P = 5.57 wt %. In the Cowboy Canyon dataset, values of over 1 wt % occur exclusively in a few of the oil shale beds, but peak values are not quite as high as in Buck Canyon: CC36, CC089.5, CC124.8, CC133.9, CC154, CC163, and CC187.

Anomalous Elemental Peaks: Uranium, Thorium, Strontium, Barium

Uranium is present as a trace element in all three sections: Gate, μ = 4.65 ppm, M = 2.8 ppm; Buck, μ = 8.31 ppm, M = 3.3 ppm; Cowboy, μ = 6.62 ppm, M = 3.8 ppm. As with the P data, median values increase eastward and are consistently below the mean value due to significant enrichment in just a few samples, e.g., BC43.5 has the highest recorded U at 93.4 ppm. Thorium is similar: Gate, μ = 7.04 ppm, M = 5.4 ppm; Buck, μ = 11.8 ppm, M = 6.2 ppm; and Cowboy, μ = 8.74 ppm, M = 5.7 ppm, with a peak reading of 153 ppm in BC152. Enrichment of both elements, where it occurs, is in most every aforementioned phosphatic oil shale bed from all three sections, a pattern confirmed when the data are normalized against Si (appendices II to IV and figure 7). There is also enrichment to some degree in the evaporitic shale interval of Buck Canyon and Cowboy Canyon, but it is stressed that not all phosphatic oil shale beds are enriched in both of these elements: GC31 has Th but not U enrichment; GC18, GC50.8, and GC130 have U, but not Th enrichment; and GC61.5 lacks both U and Th enrichment; whereas BC31.5, BC43.5, BC61.1, BC77.5 and CC89.5 have U but not Th enrichment, and BC65.5 and CC36 are not enriched in either element. There does not seem to be any stratigraphic pattern to such a distribution. Accepting the limitations of any statistical analysis of the datasets, centered log-ratio transformations nevertheless suggest high covariances of P, U and Th and a positive correlation with each other (figure 8).

Strontium is another element that, in several phosphatic oil shale and evaporitic shale beds, exhibits enrichment. However, the peaks are not as pronounced (appendices II to IV, and figure 7), and log-ratio covariances for the entire sections are not as strongly positive. Values for Sr are also notably impoverished in several of the tuff beds (GC63, GC72.9, GC238.6, BC51.4, BC143, BC160.5, and in the tuffaceous sandstone at BC172 and overlying CC149, CC172) yet enriched in the GC224 tuffaceous sandstone.

Barium values are elevated in several phosphatic oil shale beds in Cowboy Canyon, most notably in CC124.8, although the enrichment is greatest in the next sample upsection, CC128, an evaporitic shale (7321 ppm, μ = 705.6 ppm). In Buck Canyon, where μ = 830 ppm and M = 528 ppm, both BC77.5 and BC128.2, from phosphatic oil shale, show elevated values of over 950 ppm, although the greatest enrichment occurs in a sandstone (BC37.5, 2829 ppm) and the muddy mud-pebble conglomerate (BC14, 20,780 ppm, or 2.0 %). By contrast, in Gate Canyon (μ = 600 ppm, M= 551 ppm) the greatest enrichment is associated with the Wavy Tuff (72.9 m, 2073 ppm), and none of the phosphatic beds exhibit elevated Ba values.

Anomalous Elemental Peaks: Rare Earth Elements

There are several REE anomalies identified in the three sections, and the enrichments are more common and more pronounced in the heaviest REEs (including yttrium), to the point that they can be more abundant than atomically lighter lanthanoids (appendices II to IV, and figure 7B). Once again, there is an affinity for such peak values to be associated with the oil shale and evaporitic-shale beds, particularly where such beds are phosphatic (figure 7B). For example, Yb (76) is equally or more abundant than Sm (68) in the oil shale samples GC50.8, GC91.4, and GC130; BC31.5, BC43.5, BC61.1, BC77.5, and BC128.2; CC8.2, CC64, CC124.8, CC133.9, and CC178. The abundance reversal is also present in the GC07 shale and GC224 tuffaceous siltstone. Conversely, abundance of the light REEs such as Ce often peak in other facies (e.g., GC22, GC40, GC168, and GC305), although such trends are only apparent in Si-normalized data for BC14, BC37.5, and BC176. The behavior of the REEs is further discussed below.

Anomalous Elemental Peaks: Other Elements

Abundance-depth plots of the major metal oxides (Fe, Mn, Ti; appendices II to IV) show a generally irregular distribution and, although arenaceous samples GC22, GC40, and GC176 in Gate Canyon show somewhat higher than average values, it is more difficult to visually pick out any enrichments in the other canyons. Furthermore, when normalized to Si, even these peaks disappear. Instead, Si is generally enriched relative to the three metals in the arenaceous sample BC37.5, and relative to Mn and Ti in the tuffaceous samples BC51.4 and GC 72.9 (Wavy Tuff). The other relatively abundant period 4 transitional metal, V, exhibits irregularly higher than average values in the different sections.

With respect to the other group 3 transition metals, Zr and Hf, peak abundances are less pronounced eastward. At Gate Canyon, many of the arenaceous and tuffaceous rocks have elevated Zr and Hf values, with samples GC72.9, GC200.8, and GC238.6 being most pronounced. The latter two remain quite distinct when the data are normalized. At Buck Canyon, samples from the three major sandstone intervals (BC126, BC172, BC 176, BC208, BC212, and BC216) all exhibit enrichments that are still present in the Si-normalized plots. At Cowboy Canyon, only the

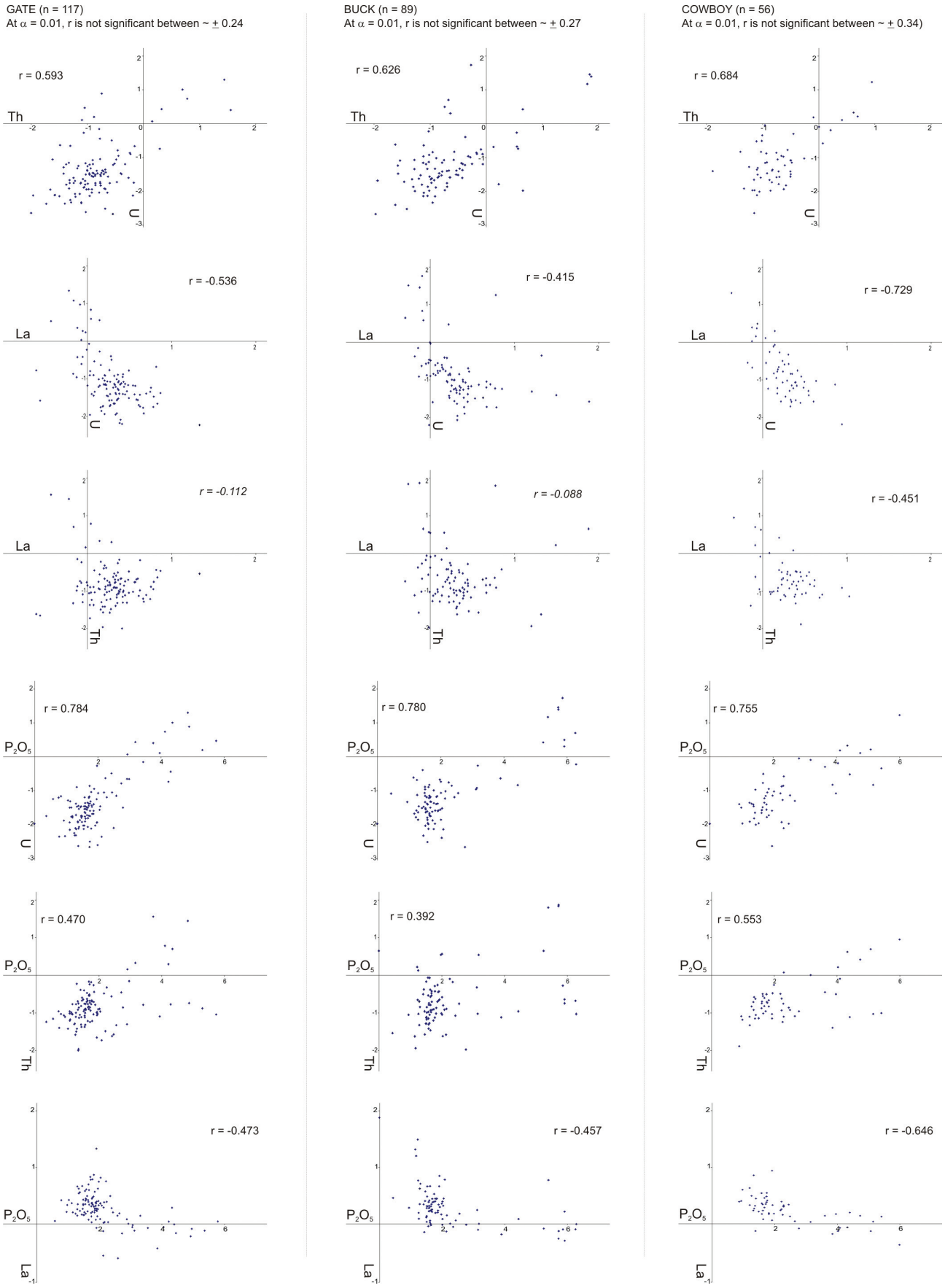

Figure 8. *Scatter plots of elements P, La (representing the REEs), Th, and U after centred log-ratio transformations (following Aitchison, 1986; Davis 2002) for all data in Gate, Buck, and Cowboy Canyons. Correlation coefficients have been added that indicate significance at α = 0.01 for all plots except La:Th in Gate and Buck Canyons, but since samples were not randomly collected (see discussion in text) caution is advised regarding their statistical validity.*

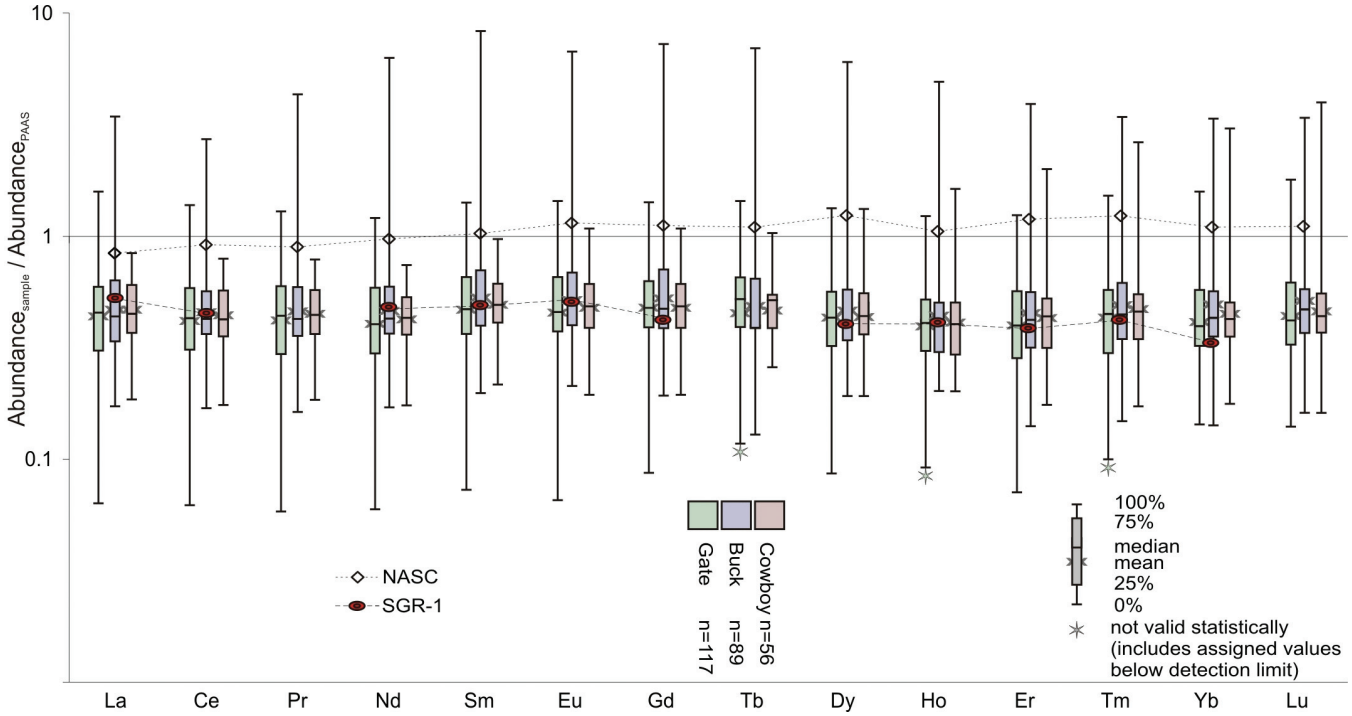

***Figure** 9. Summary statistics of the rare earth elements at Buck, Gate, and Cowboy Canyons expressed as box-whisker spider plots of abundance against Post-Archean Average Australian Shale (PAAS; Taylor and McLennan, 1985; McLennan, 1989). Equivalent values for the NASC composite (Gromet and others, 1984) and the USGS reference material SGR-1 (USGS website, 2010) are included for comparison and illustrate that most samples plot very close to the SGR-1 standard.*

tuffaceous sandstone CC149 is enriched, and even these peaks disappear in Si- normalized depth plots. Normalization also indicates relative Si enrichment in BC67.3, GC04, GC18.2, and GC247.9. The other group 4 transition metals, Nb and Ta, have similar tendencies.

In all three canyons, many of the remaining transition and post-transitional metals commonly occur at levels below what could be detected by the chosen analytical method. Regardless, in isolated samples from various facies in Gate Canyon, elemental abundances are high (appendices II to IV) and are worthy of mention. The non-phosphatic oil shale GC0.0 is highly enriched, relative to other samples, in Pb (375 ppm), Zn (610 ppm), As (323 ppm), and Sb (3.7 ppm); for GC24, a sandstone, values are even higher (GC22.0 and GC26.4, from adjacent arenaceous siltstone, are similarly elevated): Pb = 1170 ppm, Zn = 1100 ppm, As = 464 ppm, and Sb = 7.3 ppm. In addition, the siltstone GC204 has peak Sb (25.8 ppm) as well as high As (141 ppm). In contrast, for Buck Canyon the BC61.1 oil shale contains the highest values for Zn (110 ppm) and Sb (3.5 ppm), whereas Pb peaks at 30 ppm in a tuff (BC143) and As at 130 ppm in a sandstone (BC212). Peak values in Cowboy Canyon are similar or even lower.

PAAS-Normalized Spider Plots: REEs

PAAS-normalized spider plots of the lanthanoids (appendices V to VII) allow for further insight into their variable distribution in the three datasets. Almost all samples plot at values impoverished relative to PAAS (figure 9), and in most cases all lanthanoids are equally deficient, resulting in a flat profile similar to the SGR-1 standard, particularly shale samples from the MOSZ (from where SGR-1 has been taken in the Piceance Creek Basin). Samples that display a negative Eu anomaly (e.g., sandstones BC172, BC176, and BC216) were samples most likely taken from a more weathered surface, since this is the REE that is most mobile under surface conditions (Hollings and Wyman, 2005).

Although most samples display a flat profile, other patterns are present, usually associated with phosphatic oil shale and tuff or tuffaceous sandstone. For example, a few phosphatic oil-shale beds display a gradual enrichment from lightest to heaviest REE. In the case of the samples CC124.8 and BC128.2 (both replicates), the gradual enrichment becomes so pronounced that elements Tb and heavier have abundances higher than the PAAS standard (figure 10). This was also the same pattern encountered in what is believed to have been the same phosphatic oil shale bed at Buck Canyon in the preliminary study. Other phosphatic oil-shale samples exhibit a dog-leg (or hockey-stick) profile, with a relatively flat profile through the light REEs and then a steeper gradient in the middle and heavy REEs. For GC50.8 and BC43.5, the slope break occurs at Tb, whereas for GC130 and BC77.5, the change is at Ho (figure 10).

Tuffaceous samples are highly variable: there are isolated profiles with a gradual decrease in the abundance of pro-

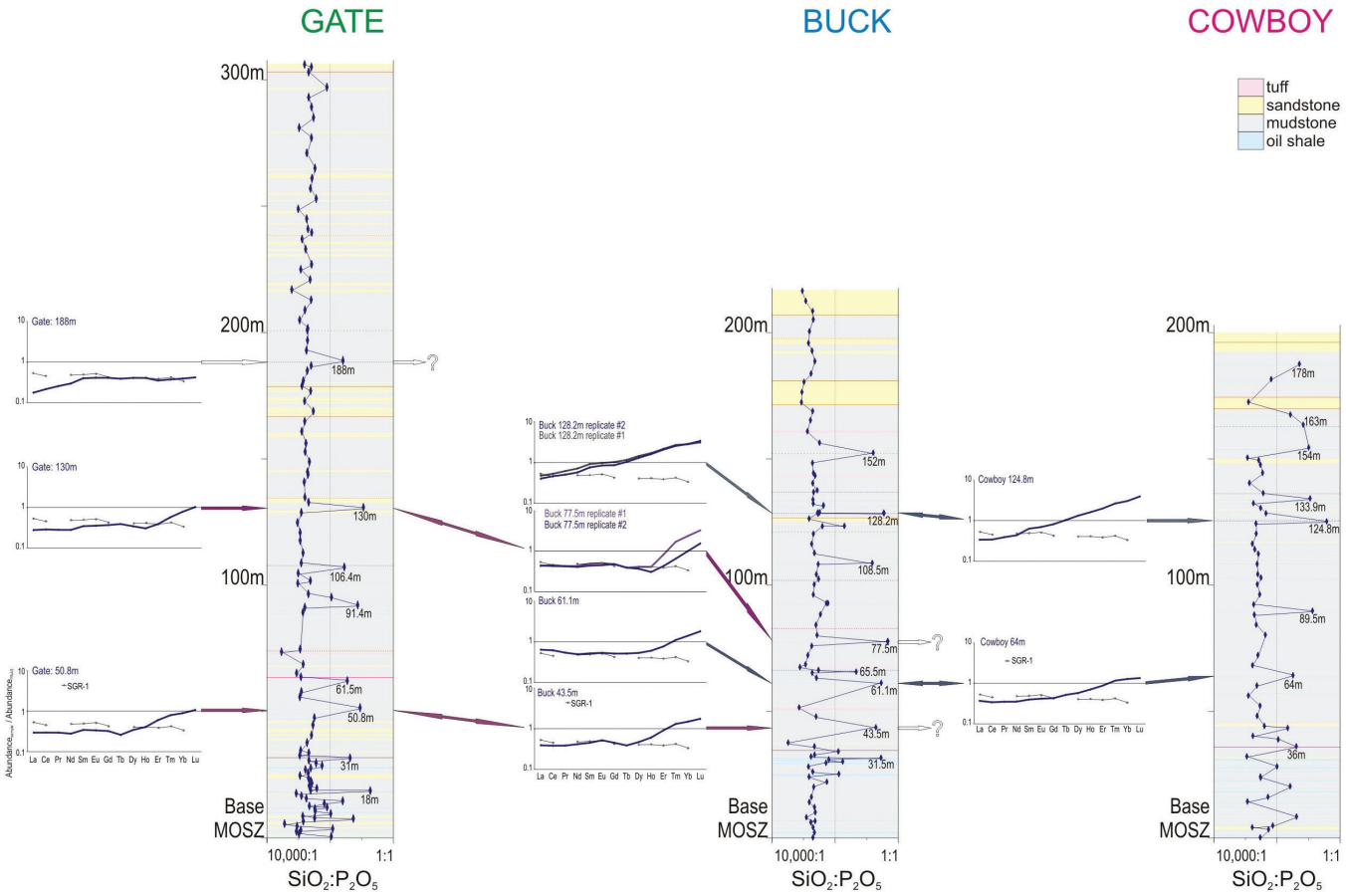

Figure 10. *Selected spider plots of phosphatic oil shale samples at Buck, Gate, and Cowboy Canyons. Note the same dog-leg seen in the two replicates of the Buck Canyon 77.5 m sample (flat profile from La to Ho; steep increase in relative abundance from Ho to Lu) is also present in the 130 m sample from Gate Canyon.*

gressively heavier REEs with respect to PAAS (e.g., BC176), but most commonly there is a relative enrichment in the middle REEs resulting in a convex-upward or near omega-shaped profile (e.g., BC37.5, GC74); yet others are a composite of the above profiles (e.g., GC72.9) and others have a very irregular, jagged profile (e.g., BC172). Sandstone, variably tuffaceous, may also exhibit a ubiquitous enrichment or impoverishment (e.g., BC172 and GC304, respectively) across the entire REE spectrum.

General Depth Trends

The preceding assessments of the data have indicated that numerous elements preferentially associate with particular facies; for example, P, Th, U, Sr, and the REEs associate with oil shale, whereas Fe, Mn, Ti, Zr, Hf, Nb, and Ta associate with tuff and sandstone. Thus, for the latter group of elements, simple depth-abundance plots (appendices II to IV) tend to show increasing amounts upsection because sandstone is more commonly sampled upsection. Visual trends are also affected by the targeting of oil shale beds in the supplementary sampling program (hence the plotting of both "all data" points and just the "systematic" samples on the same depth plot in the appendices). Accordingly, in assessing other trends in the data (gradual/sharp increases/decreases with increasing height in the section), the subsequent analysis focuses exclusively on the samples from the carbonate mudstone-shale facies. Additionally, elemental ratios have already been plotted for various elements (P, U, Th, etc.) against Si in order to assess the results without concern for closure of the data. This process can be extended to assess the variability between any two other elements. Over 150 of these ratio-depth plots have been assessed for each of the three locations. Several plots exhibit some sort of pattern, but only the following trends are considered worthy of further note.

When plotted against either Si or Al, the elements Mg, K, and Na in Buck and Cowboy Canyons exhibit a slight change in abundance upsection: the latter element tends to increase, the other two to decrease (figure 11). Such trends are not discernable in Gate Canyon. Conversely, plots of Si or Al against Ca may show a slight decrease in Gate but a slight increase in Cowboy, with nothing discernible in the Buck Canyon database. A ratio-depth plot of Mg:Ca also displays a drop in Mg abundance at different elevations in Gate and Buck: the lower ratio occurs above the ~195 m elevation in Gate Canyon, above ~75 m elevation in Buck Canyon, and persists throughout the Cowboy Canyon section (figure 11A).

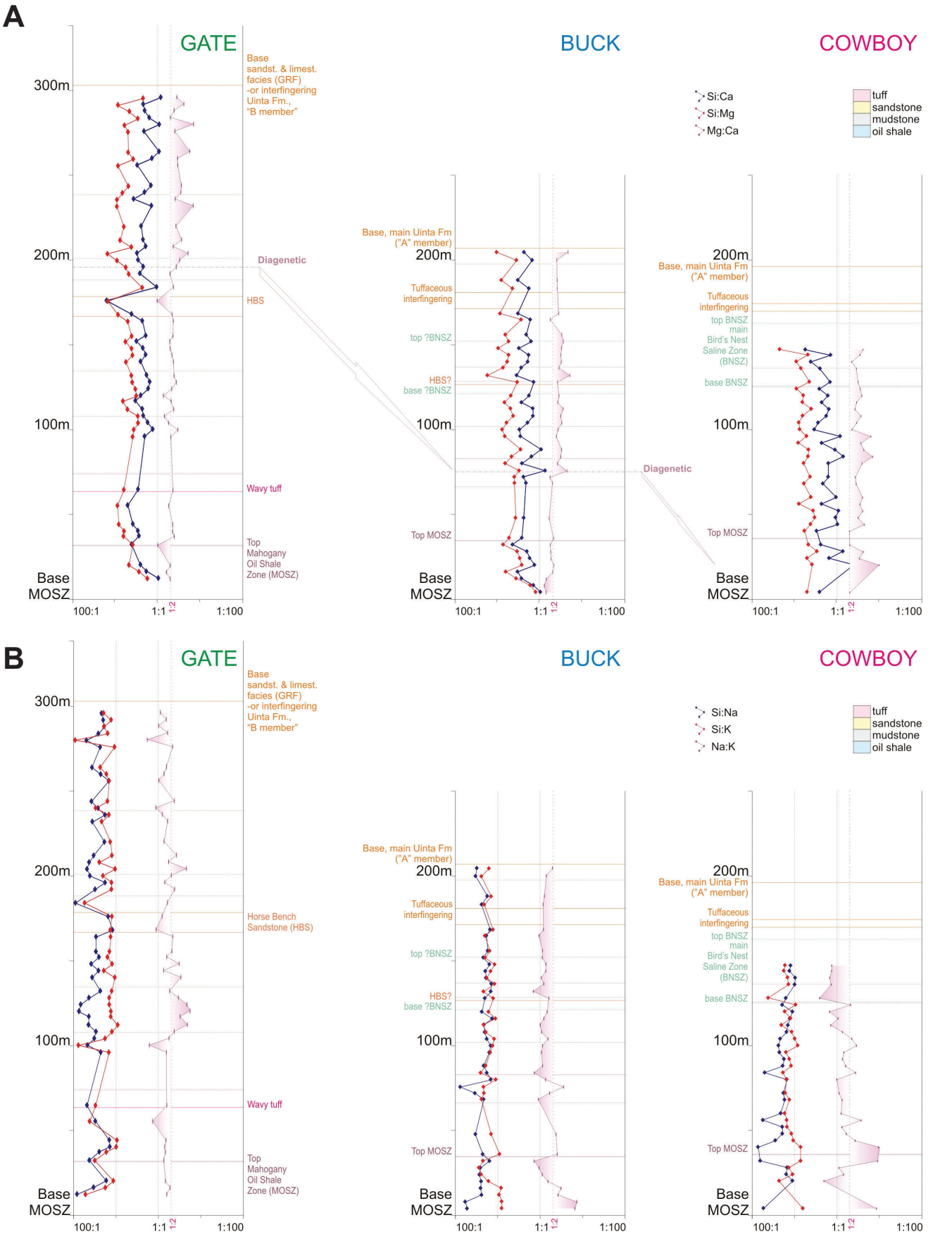

Figure 11. *Ratio-elevation plots at Buck, Gate, and Cowboy Canyons for (A) silicon against magnesium and calcium, and magnesium:calcium, (B) silicon against sodium and potassium, and sodium:potassium, (C) thorium:uranium, and (D) silicon:cesium. In the plot of the Mg:Ca ratio in 11A, note the increased Mg content below GC200 and BC75 m. The top of this interval crosses surface-correlated beds and is likely diagenetic in origin.*

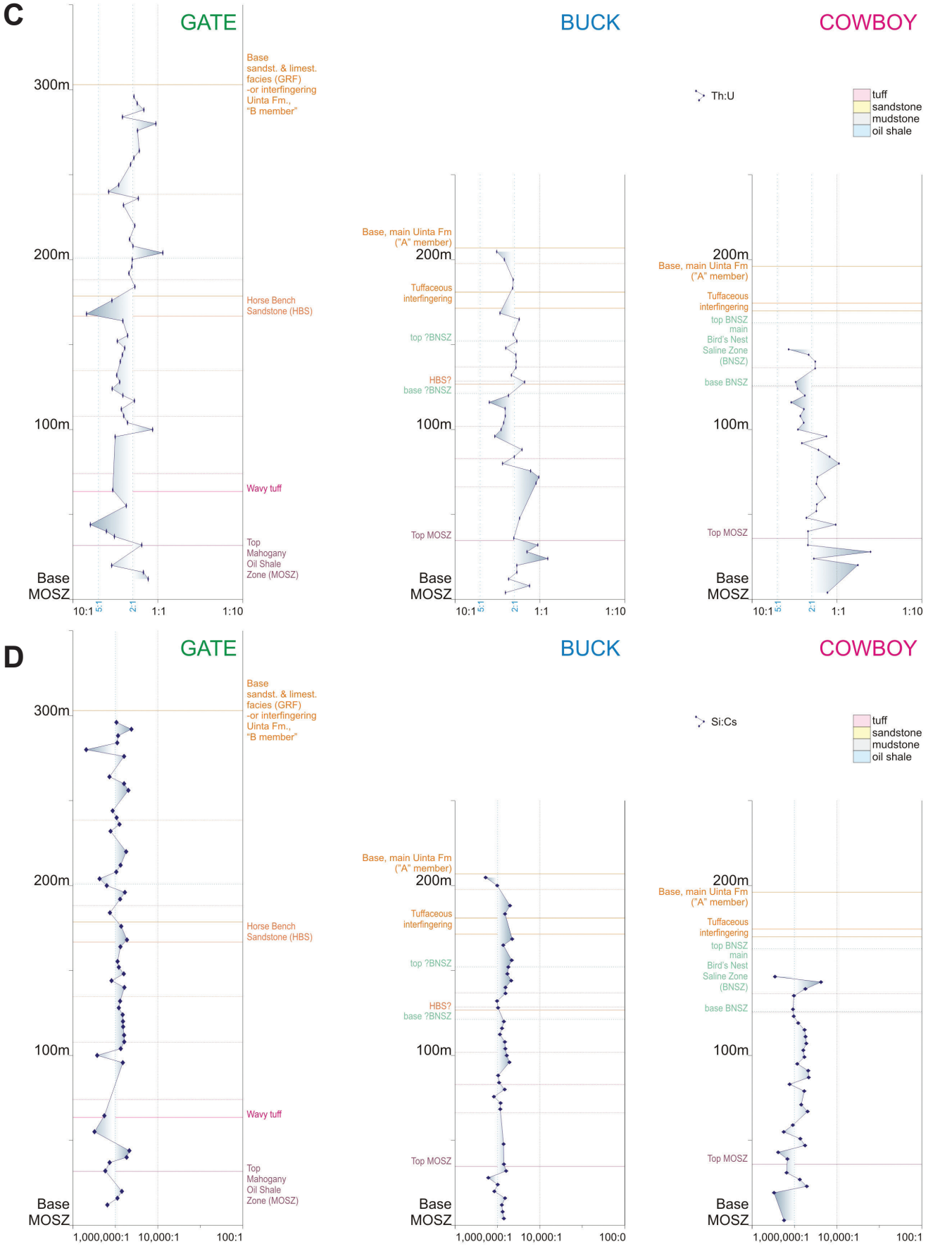

Figure 11. *Continued.*

A similar divergence in trends is seen with Th and U. An increase upsection in Th:Si occurs only in Cowboy Canyon, while U:Si shows an increase upsection in Gate Canyon and a marginal decline upsection in Buck Canyon. As a result, for the Th:U ratios there is a decrease upsection in Gate Canyon but an increase upsection in the other two datasets (figure 11C). Plots of Si against Cs only show increases upsection in Buck Canyon and Gate Canyon (figure 11D).

Geochemical Correlation

The current dataset is most promising as a correlative tool with respect to oil shale, particularly beds that are enriched in P and the heavy REEs. As shown in figure 10, generally unique profiles and abundances of REEs (relative to PAAS) would best fit with the last of the correlations discussed in the Potential Correlations section above (figure 5D). The most impressive correlation would be that of the phosphatic oil shale at 128.2 m in Buck Canyon and 124.8 m in Cowboy Canyon. Together with the correlation of samples BC61.1 and CC64, this would confirm the layer-cake stratigraphy proposed between the two canyons. In contrast, a correlation of GC50.8 with BC43.5, and a correlation of GC130 with BC77.5 requires a thickening of the Gate Canyon section relative to the sections further east, with the thickening occurring below HBS.

Geochemical correlation between tuffs and tuffaceous sandstones between localities also supports a thickening to the west between the Buck and Gate Canyon localities. Tuff and tuffaceous sandstone, as previously noted, exhibit widely varying spider-plot profiles. So far, only a few tuffs have been analyzed and it is uncertain if they can be a positive tool for correlation: no profiles are confidently reproduced in different datasets. However, two tuffaceous sandstone samples from Cowboy Canyon (CC149, CC172) more closely resemble the tuff and tuffaceous sandstone samples in Buck Canyon (BC143, BC160.5, BC172, BC176) than what is considered to be the HBS (BC126, figure 12). Similarly, the spider plots of the HBS samples at Gate Canyon (GC134, GC168) more closely resemble the profile of BC126 than the overlying samples in Buck Canyon. Such profiles again fit better with a stratigraphy that has the Gate Canyon succession thicker above MOSZ relative to the more eastern successions. An unfortunate limitation to the correlation of other tuff beds in the current report is that several have only been sampled and analyzed in one dataset. For example, Wavy Tuff (GC72.9), and what is thought to be the S2 marker (BC37.5), have very distinctive spider-plot profiles (figure 12) with GC72.9 also having a unique Ba enrichment, elevated Zr, Hf, and impoverished Mn and Ti values.

There are also a few possible reasons why geochemical signatures of oil shale beds can only be correlated at two out of three localities. This may be a function of any of four factors:

(i) A particular oil shale may not extend through all three outcrops, either through truncation or pinch-out.

(ii) A particular oil shale may be present at all three sections, but it may not have been sampled in every case, either due to the sampling procedure or lack of exposure of the particular oil shale.

(iii) A particular oil shale may be sampled at all three sections, but correlation is not made because of within-bed lateral variation; the profile of the spider plot varies spatially for any particular oil shale due to differing precipitative or diagenetic conditions, making any correlation uncertain.

(iv) A particular oil shale may be sampled at all three sections, but correlation is not made because of within-bed vertical geochemical variation and the sampling of different stratigraphic levels within an oil shale; the P enrichment in BC128.2 is not present in the sample from lower in the same bed (BC128.1) and so even sampling different thicknesses of a bed could cause considerable variation.

In contrast to the above correlations, the distinct upsection change in Mg:Ca ratios from Mg-enriched to Mg-depleted in both Gate Canyon and Buck Canyon is an example of a correlation that would have to cross surface marker beds (figure 11A). In this case, however, the correlation may still be appropriate, but mark the effect of a regional deep- or late-diagenetic event. The boundary dips downsection toward the east, which would suggest, if it were originally a paleohorizontal boundary (it may not have been), a downwarping of the east or uplift of the west subsequent to the diagenetic event.

XRD RESULTS SUMMARY

The occurrence of anomalously high phosphorus readings in the ICP data and the association, in most cases, with oil shale, raises the question as to the mineralogical occurrence of the element. To answer this question, 17 of the Buck Canyon samples, comprising 10 oil shale, 6 mudstone, and 1 sandstone (appendix VIII), were selected for further investigation by XRD analysis.

XRD analyses confirm the presence of phosphate in oil shale from BC77.5, BC108.5, and BC128.2, as well as in the gray evaporitic shale from BC152 (note that the calculated percentages tabulated in the appendix reflect the abundance exclusive of the organic phase) and, specifically, that for each sample, calcium fluorapatite (CFA) is the phosphate mineral (figure 13A). The BC128.2 sample uniquely has a very low dolomite component whereas BC77.5 is low in all carbonate phases, high in feldspar, and negligible quartz. Note that the analyses also confirm that the so-called mudstone of the upper GRF actually comprises a predominance of carbonate phases, with the silicon-bearing minerals collectively subordinate, and clay minerals

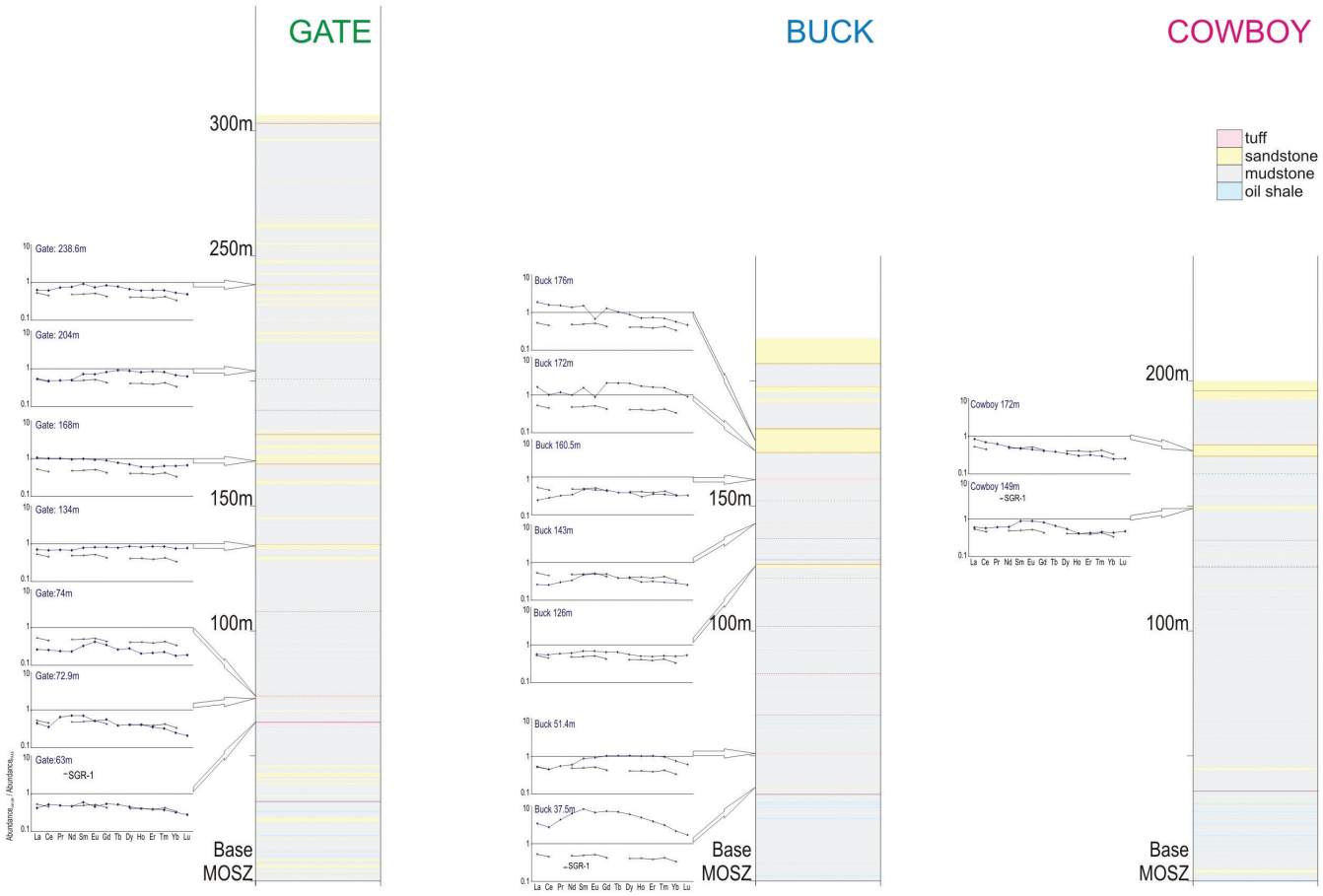

Figure 12. *Selected REE spider plots of tuff and tuffaceous sandstone samples at Buck, Gate, and Cowboy Canyons.*

(included in the sheet-silicates [mica] column of appendix VIII) generally undetectable. No pyrite was detectable in any sample, although in BC131 (figure 13B), a peak radiation occurs at 33.07° ($2\theta_{Cu}$), which is usually indicative of pyrite. However, other distinguishing pyrite peaks at 37.10°, 40.79° and 56.34° are absent, so the origin of the 33.07° peak is unclear.

SEM RESULTS SUMMARY

Materials from two oil shale samples (BC128.2, BC131) and an evaporitic shale (BC152) have been analyzed using SEM to determine the nature of the more atypical mineral phases, particularly the CFA. Sample surfaces were viewed both along sections perpendicular to bedding and along bedding surfaces.

The CFA in BC128.2 and BC152 is found to be pervasive across the observed bedding surface, typically as micron-scale small crystals in the shale matrix; no CFA was found in BC131. In BC128.2, concentrations of microcrystalline CFA are also identified fossilizing coccoidal organic matter (figure 14A, B). The origin of the fossils is uncertain: possibly a species of green alga (e.g., Pediastrum) that was buried and quickly fossilized before it degraded, or a species of shallow-substrate bacterium. The collection of EDS data recovered from a transect from the core to the rim of a fossil coccoid (figure 14C) further indicates that the archetypal formula for CFA holds true for these crystals:

$$Ca_{10-a-b-c}\,Na_a\,Mg_b\,(PO_4)_{6-x}\,(CO_3)_{x-y-z}\,(CO_3,F)_y\,(SO_4)_z\,F_2$$

where 2c = x – y – a = vacancies in the Ca site. The Ca:P ratio is the expected apatite ratio of 1.67 (r = 0.959), although the F:P ratio is anomalously low. The gradual reduction, stoichiometrically, in Ca abundance from the center to the rim of the fossil alga correlates with increased Na, no doubt due to lattice substitution. The reduction in S and P abundance from center to rim is mitigated by increased F content that would also counter charge imbalances in the lattice (figure 14C).

Various other minerals have been identified from elemental mapping of the three samples, including quartz, various feldspars, various micas, calcite, dolomite, zircon, rutile, sphalerite, barites-celestine, and pyrite.

DISCUSSION

It is not the purpose of this report to provide a detailed geological explanation for the chemical variations: this will

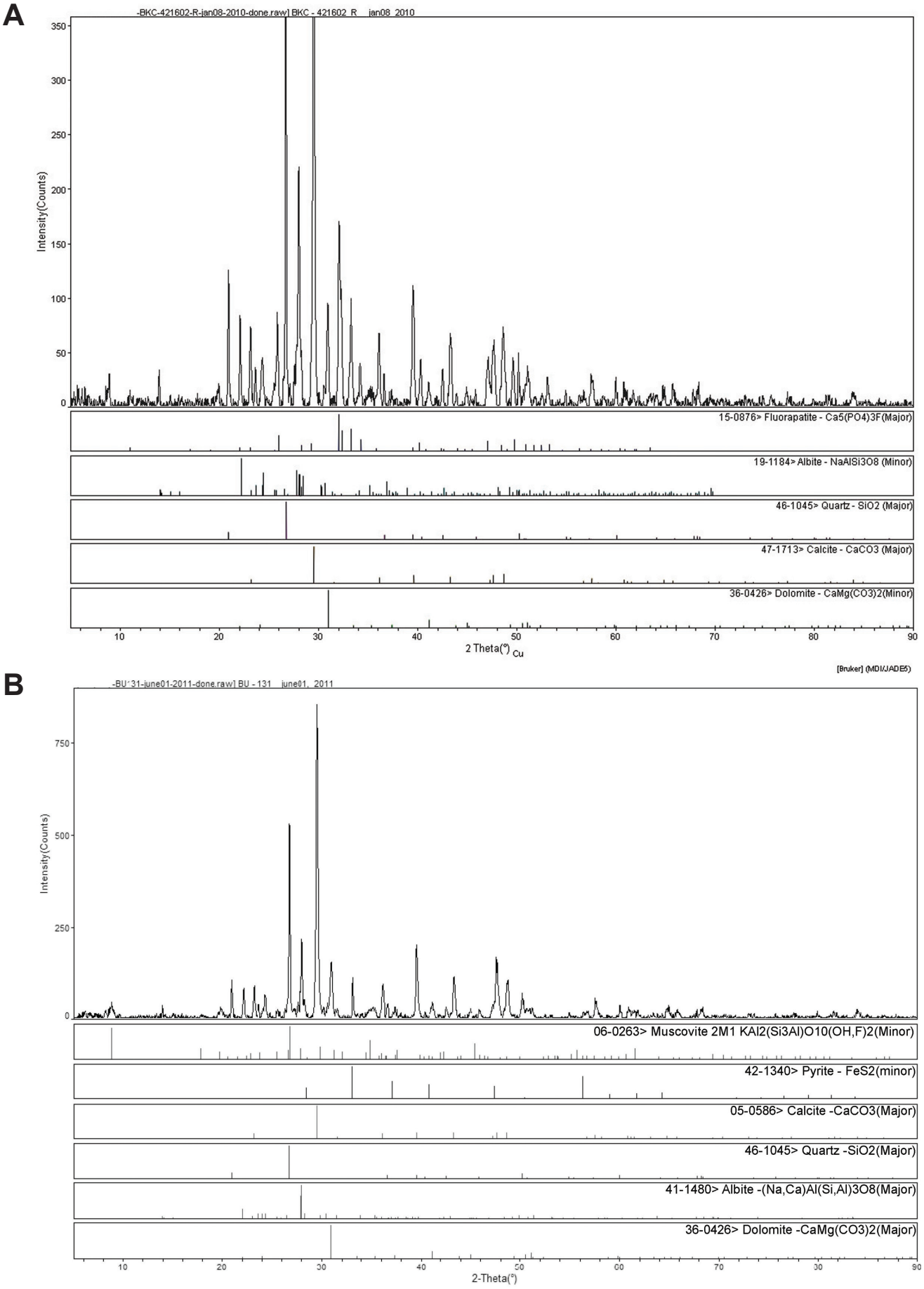

Figure 13. *X-ray diffractometer traces of selected samples from Buck Canyon. (A) BC128.2 m, (B) BC131 m.*

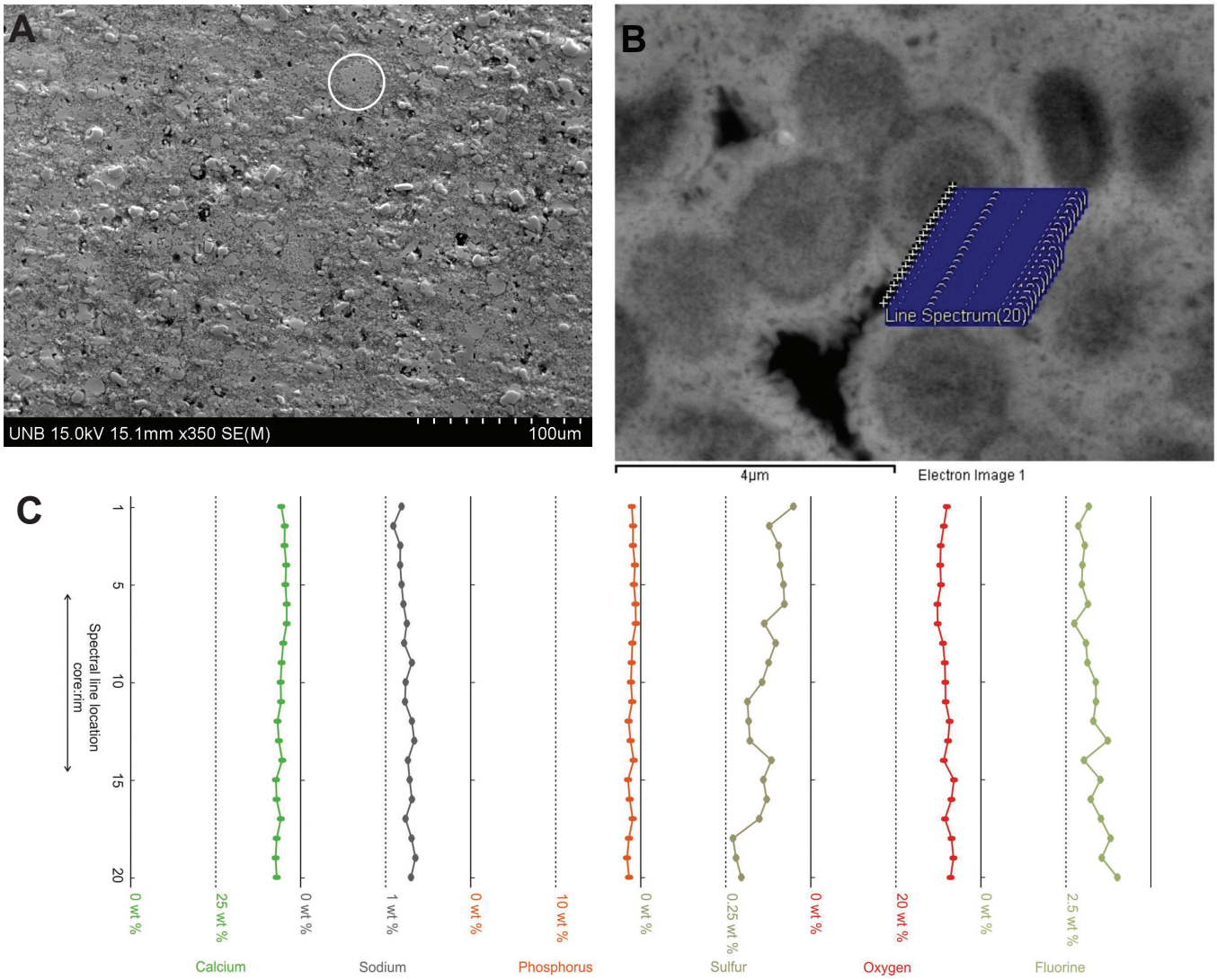

Figure 14. *SEM images of a bedding surface in the oil shale at 128.2 m in the Buck Canyon section. (A) Circled is what might be interpreted as a large fossilized coccoid. The fossilizing calcium fluorapatite crystals are typically less than 1 µm in length, but crystals may reach 3 µm where they have formed part of the groundmass. (B) Detail of a "fossilized coccoid". The location of 20 EDS analyses forming a transect from the center (#1) to the outer rim (#20) of a coccoid is also shown. (C) Stoichiometric plots taken from the 20 EDS analyses.*

be done in other planned research articles. Nonetheless, a brief overview is provided. The well-preserved nature of the fossil coccoids, and the incorporation of progressively less SO4 into the CFA lattice of fossilizing crystals, argues for a very early diagenetic phosphatizing event, probably in the very shallow substrate in the sulfate reducing zone. The phosphorus cycle, as it applies to the initial accumulation and concentration of organic phosphorus in the substrate (and hence the association of P with oil shale) is well understood (Föllmi, 1996; figure 15). Most likely, organic P and previously dissolved P adsorbed onto clays, carbonates, and ferric hydroxides remobilize to form dissolved interstitial phases. Under anoxic conditions this P may normally diffuse into the overlying water column by various (bio-) geochemical mechanisms (see review by Wetzel, 2001), but if sulfate concentrations also increase, anion exchange reactions drive more P into solution (Caraco and others, 1993), potentially to the point of supersaturation, and CFA precipitates rapidly through nucleation and crystallization on mineral surfaces or biological soft and hard parts (Föllmi, 1996). Dissolved REEs may be adsorbed onto organic matter in surface waters—carbonate complexing is important for organic lanthanoids—or scavenged by apatite (the REEs again substituting for Ca) associated with organic detritus (Brookins, 1989; Bozau and others, 2008). Such anoxic conditions also favor the accommodation of tetravalent uranium, in lieu of calcium, in CFA (Altschuler and others, 1958).

CONCLUSIONS

A preliminary chemostratigraphy of the upper GRF appears workable based on ICP measurements taken from three sampled and separately analyzed datasets from Gate

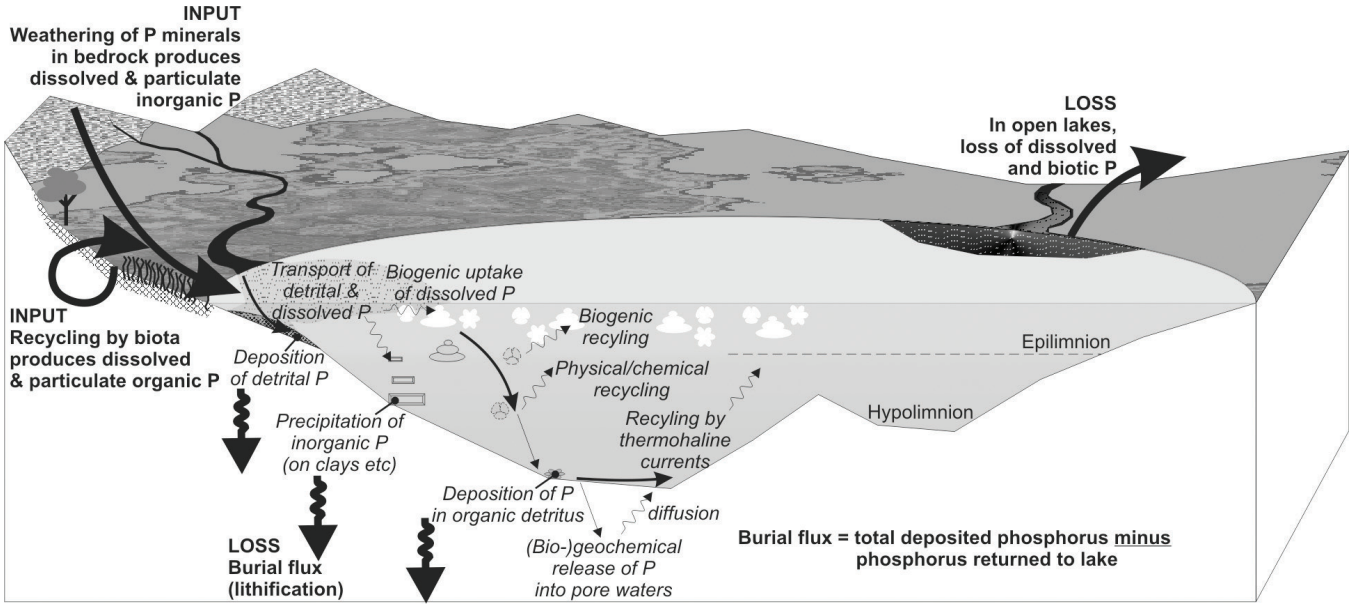

Figure 15. *The phosphorus cycle in lakes.*

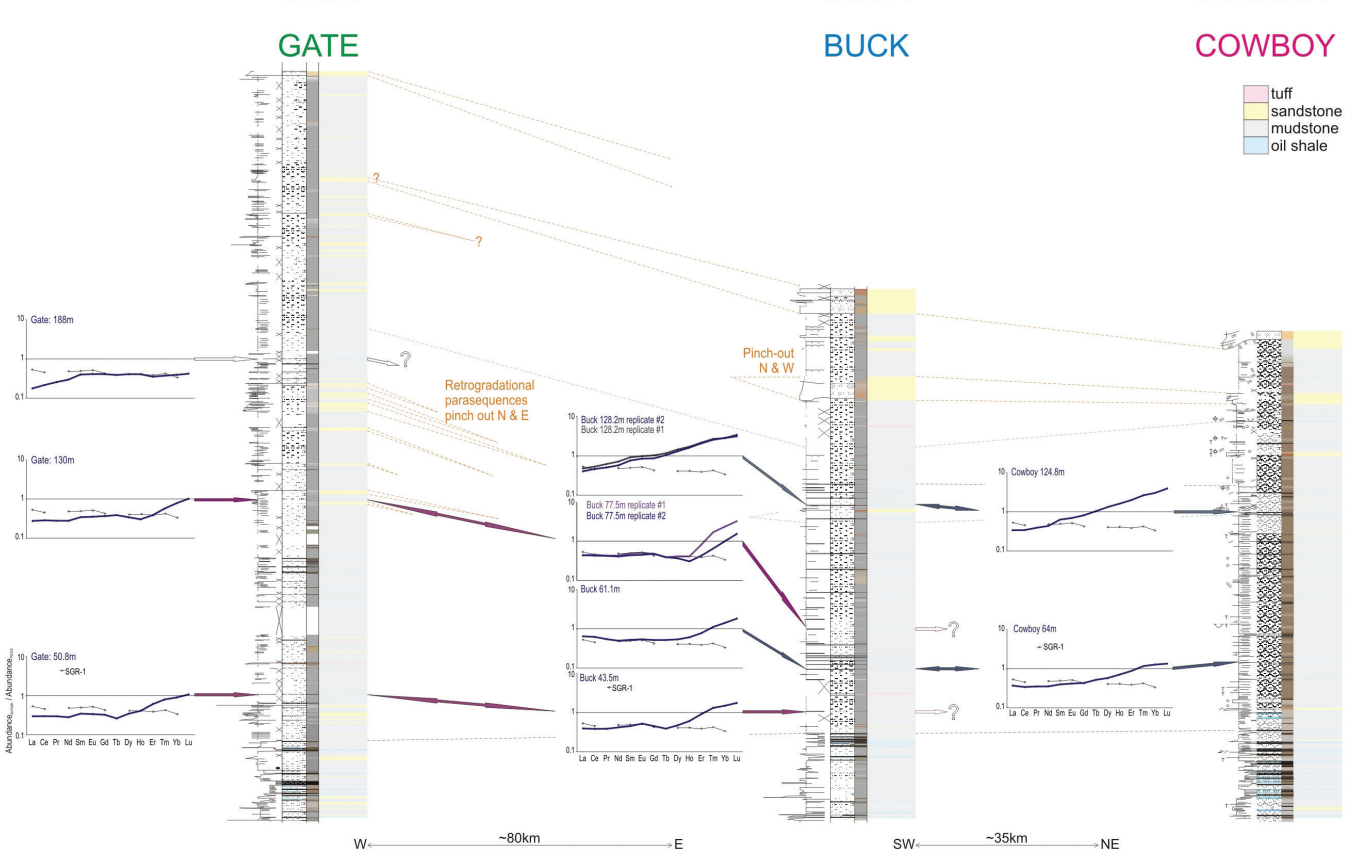

Figure 16. *Currently preferred correlation of strata at Buck, Gate, and Cowboy Canyons, combining parts of figure 5D and figure 10.*

Canyon, Buck Canyon, and Cowboy Canyon. In particular, correlation of oil shale beds with elevated P and associated heavy REE values and REE signatures from tuffaceous sandstones supports a correlation scheme that displays significant thickening to the west at Gate Canyon relative to the Buck Canyon and Cowboy Canyon sections in the east (figure 16).

Since the P, U, and REE anomalies are considered related to very shallow subsurface diagenesis, they can reasonably be equated to syndepositional time lines, and apatite's subsequent mineralogic stability makes these elements useful chemostratigraphic tools. Later, deep-burial diagenesis most likely was the cause of variation in the Mg:Ca ratio. Enrichment of deeper pore waters in Mg^{2+}

may come from several sources (Scoffin, 1987): from clay-mineral transformations in adjacent or underlying formations (since clays are rare in the upper GRF), or alteration of algal filaments being the most likely. Such diagenetic effects need not follow depositional surfaces (time lines and marker beds) or facies boundaries, leading to the observed "inclined" boundary between the higher Mg:Ca and overlying lower Mg:Ca ratio. Although factual boundaries, they are of limited chemostratigraphic utility.

ACKNOWLEDGMENTS

Funding for this project was courtesy of the Utah Geological Survey (UGS), State of Utah Petroleum Research Grant, with additional support from a Canadian Natural Science and Engineering Research Council (NSERC) Discovery Grant to the PI. Michael Vanden Berg and Craig Morgan (UGS) are thanked as the contact personnel relating to the UGS grants and for continuing discussion, together with Doug Sprinkel (UGS), on geological matters relating to the Uinta Basin. Field assistance and lab sample preparation were provided by University of New Brunswick (UNB) students Daniel McIsaac, Nicola Harcourt, and Adam Clowater. XRD analysis was undertaken by Ven Reddy (UNB), SEM chips and thin sections were prepared by Ancel Murphy and Calvin Nash (UNB), and SEM analysis was supervised by Suporn Boonsue at the PASSC facility in the Department of Earth Sciences at UNB. Activation Laboratories (Ontario, Canada) provided the ICP analyses. Finally, Mary and Steve McPherson (McPherson Geologic Consulting Ltd) are thanked for hosting Nicola and Adam during their 2008 field season. Lauren Birgenheier (University of Utah) and Michael Vanden Berg (UGS) are thanked for their constructive reviews of this manuscript.

REFERENCES

Aitchison, J., 1986, The statistical analysis of compositional data: Chapman and Hall, New York, 416 p.

Altschuler, Z.S., Clarke, R.S., and Young, E.J., 1958, Geochemistry of uranium in apatite and phosphorite: U.S. Geological Survey Professional Paper 314-D, 90 p.

Birgenheier, L.P., and Vanden Berg, M.D., 2011, Core-based integrated sedimentologic, stratigraphic, and geochemical analysis of the oil shale bearing Green River Formation, Uinta Basin, Utah: DOE Topical Report.

Boyer, B.W., 1982, Green River laminites—does the playa-lake model really invalidate the stratified lake model?: Geology, v. 10, p. 321–324.

Bozau, E., Göttlicher, J., and Stärk, H-J., 2008, Rare earth element fractionation during the precipitation and crystallisation of hydrous ferric oxides from anoxic lake water: Applied Geochemistry, v. 23, p. 3473–3486.

Bradley, W.H., 1973, Oil shale formed in desert environment—Green River Formation, Wyoming: Geological Society of America Bulletin, v. 84, p. 1121–1124.

Bradley, W.H., and Eugster, H.P., 1969, Geochemistry and paleolimnology of the trona deposits and associated authigenic minerals of the Green River Formation of Wyoming: U.S. Geological Survey Professional Paper 496-B, 71 p.

Brookins, D.G., 1989, Aqueous geochemistry of rare earth elements: Reviews in Mineralogy, v. 21, p. 201–225.

Bryant, B., 1992, Geologic and structure maps of the Salt Lake City 1° x 2° quadrangle, Utah, and Wyoming: U.S. Geological Survey Miscellaneous Investigations Series Map I-1997, scale 1:125,000.

Caraco, N.F., Cole, J.J., and Likens, G.E., 1993, Sulfate control of phosphorus availability in lakes: Hydrobiologia, v. 253, p. 275–280.

Cashion, W.B., 1967, Geology and fuel resources of the Green River Formation, southeastern Uinta Basin, Utah and Colorado: U.S. Geological Survey Professional Paper 548, 48 p.

Cashion, W.B., and Donnell, J.R., 1974, Revision of the upper part of the Green River Formation, Piceance Creek Basin, Colorado, and eastern Uinta Basin, Utah: U.S. Geological Survey Bulletin B-1396-G, 9 p.

Dane, C.H., 1954, Stratigraphic and facies relationships of the upper part of the Green River Formation and lower part of the Uinta Formation in Duchesne, Uintah, and Wasatch Counties, Utah: American Association of Petroleum Geologists Bulletin v. 38, p. 405–425.

Dane, C.H., 1955, Stratigraphic and facies relationships of the upper part of the Green River Formation and lower part of the Uinta Formation in Duchesne, Uintah, and Wasatch Counties, Utah: U.S. Geological Survey Oil and Gas Investigation Chart 52.

Davis, J.C., 2002, Statistics and data analysis in geology—3rd Edition: New York, John Wiley and Sons, 638 p.

Desborough, G.A., 1978, A biogenic-chemical stratified lake model for the origin of oil shale of the Green River Formation—an alternative to the playa-lake model: Geological Society of America Bulletin, v. 89, p 961–971.

Donnell, J.R., 2009, Intertonguing of the lower part of the Uinta Formation with the upper part of the Green River Formation in the Piceance Creek Basin during the late stages of Lake Uinta: U.S. Geological Survey Scientific Investigations Report 2008–5237, 25 p.

Dyni, J.R., 1996, Sodium carbonate resources of the Green River Formation: U.S. Geological Survey Open-File Report 1996–729, 39 p.

Dyni, J.R., 2008, Preliminary stratigraphic cross sections of oil shale in the Eocene Green River Formation, Uinta

Basin, Utah: U.S. Geological Survey Open-File Report 2008–1220, 11 p.

Ehrenberg, S.N., and Siring, E., 1992, Use of bulk chemical analysis in stratigraphic correlation of sandstones—an example from the Statfjord field, Norwegian continental shelf: Journal of Sedimentary Petrology, v. 62, p. 318–330.

Eugster, H.P., and Hardie, L.A., 1975, Sedimentation in an ancient playa-lake complex—the Wilkins Peak Member of the Green River Formation of Wyoming: Geological Society of America Bulletin, v. 86, p. 319–334.

Föllmi, K.B., 1996, The phosphorus cycle, phosphogenesis and marine phosphate-rich deposits: Earth-Science Reviews, v. 40, p. 55–124.

Gromet, L.P., Dymek, R.F., Haskin, L.A., and Korotev, R.L., 1984, The "North American Shale Composite"—its compilation, major, and trace element characteristics: Geochimica et Cosmochimica Acta, v. 48, p. 2469–2482.

Gualtieri, J.L., 1988, Geologic map of the Westwater 30' x 60' quadrangle, Grand and Uintah Counties, Utah and Garfield and Mesa Counties, Colorado. U.S. Geological Survey Miscellaneous Investigations Series Map I-1765, scale 1:100,000.

Hollings, P., and Wyman, D., 2005, The geochemistry of trace elements in igneous systems— principles and examples from basaltic systems, *in* Linnen, R.L. and Samson, I.M., editors, Rare-element geochemistry and mineral deposits: Geological Association of Canada, Short Course Notes 17, p. 1–16.

Johnson R.C., 1981, Stratigraphic evidence for a deep Eocene Lake Uinta, Piceance Creek Basin, Colorado: Geology, v. 9, p. 55–62.

Johnson, R.C., Mercier, T.J., Brownfield, M.E., and Self, J.G., 2010, Assessment of in-place oil shale resources in the Eocene Green River Formation, Uinta Basin, Utah and Colorado: U.S. Geological Survey Digital Data Series DDS–69–BB, 153 p.

Keighley, D., Borer, J., Morgan, C., McClure, K., and Griffen, R., 2003a, Facies asymmetry in alluvial-lacustrine basins—a transect across the Uinta Basin, eastern Utah and western Colorado: AAPG Annual Convention, Salt Lake City, May, 2003, 77 + xxxiii p.

Keighley, D., Flint, S., Howell, J., and Moscariello, A., 2003b, Sequence stratigraphy in lacustrine basins—a model for part of the Green River Formation (Eocene), southwest Uinta Basin, Utah: Journal of Sedimentary Research, v. 73, p. 987–1006.

Lambiase, J.J., 1990, A model for tectonic control of lacustrine stratigraphic sequences in continental rift basins, *in* Katz, B.J., editor, Lacustrine basin exploration – case studies and modern analogs: American Association of Petroleum Geologists Memoir 50, p. 265–276.

McLennan, S.M., 1989, Rare earth elements in sedimentary rocks—influence of provenance and sedimentary processes: Reviews in Mineralogy, v. 21, p. 169–200.

Morgan, C.D., Chidsey, T.C., McClure, K.P., Bereskin, S.R., and Deo, M.D., 2002, Reservoir characterization of the lower Green River Formation, southwest Uinta Basin, Utah: Utah Geological Survey—U.S. Department of Energy DOE/BC/15103-4 OSTI No. 805237, 140 p.

Pawlowsky-Glahn, V., and Egozcue, J.J., 2006, Compositional data and their analysis—an introduction, *in* Buccianti, A., Mateu-Figueras, G., and Pawlowsky-Glahn, V., editors, Compositional data analysis in the geosciences—from theory to practice: London, The Geological Society, Special Publications 264, p. 1–10.

Pearce, T.J., Besly, B.M., Wray, D.S., and Wright, D.K., 1999, Chemostratigraphy—a method to improve interwell correlation in barren sequences—a case study using onshore Duckmantian/Stephanian sequences (West Midlands, U.K.): Sedimentary Geology, v. 124, p. 197–220.

Pearce, T., Keighley, D., Morgan, T., and Flint, S., 2008, Chemostratigraphy of cyclic lacustrine and floodplain dominated intervals, Nine Mile Canyon, SW Uinta Basin, *in* Longman, M.W., and Morgan, C.D., editors, Hydrocarbon systems and production in the Uinta Basin, Utah: Rocky Mountain Association of Geologists—Utah Geological Association Special Publication 37, p. 121–132.

Picard, M.D., 1957, Green River and lower Uinta Formations—subsurface stratigraphic changes in central and eastern Uinta Basin, Utah, *in* Seel, O.G., editor, Guidebook to the geology of the Uinta Basin: Eighth Annual Field Conference, Intermountain Association of Petroleum Geologists, p. 116–130.

Racey, A., Love, M.A., Bobolecki, R.M., and Walsh, J.N., 1995, The use of chemical element analysis in the study of biostratigraphically barren sequences—an example from the Triassic of the central North Sea (UKCS), *in* Dunay, R.E., and Hailwood, E.A., editors, Non-biostratigraphical methods of dating and correlation: London, The Geological Society, Special Publication 89, p. 69–105.

Ratcliffe, K.T., Martin, J., Pearce, T.J., Hughes, A.D., Lawton, D.E., Wray, D.S., and Bessa, F., 2006, A regional chemostratigraphically-defined correlation framework for the Late Triassic TAG-I Formation in Blocks 402 and 405a, Algeria: Petroleum Geoscience, v. 12, p. 1–10.

Ratcliffe, K.T., Wright, A.M., Hallsworth, C., Morton, A., Zaitlin, B.A., Potocki, D., and Wray, D.S., 2004, An example of alternative correlation techniques in a low accommodation setting, non-marine hydrocarbon system—the (Lower Cretaceous) Mannville Basal Quartz succession of southern Alberta: American Association of Petroleum Geology Bulletin, v. 88, p. 1419–1432.

Remy, R., 1992, Stratigraphy of the Eocene part of the Green River Formation in the south-central part of the Uinta Basin, Utah: U.S. Geological Survey Bulletin B 1787-BB, p. BB1-BB69.

Rowley, P.D., Hansen, W.R., Tweto, O., and Carrara, P.E., 1985, Geologic map of the Vernal 1° x 2° quadrangle, Colorado, Utah, and Wyoming: U.S. Geological Survey Miscellaneous Investigations Series Map I-1526, scale 1:250,000.

Ruble, T.E., and Philp, R.P., 1998, Stratigraphy, depositional environments, and organic geochemistry of source rocks in the Green River Petroleum System, Uinta Basin, Utah, *in* Pitman, J.K., and Carroll, A.R., editors, Modern and ancient lake systems—new problems and perspectives: Utah Geological Association Publication 26, p. 289–328.

Scoffin, T.P., 1987, An introduction to carbonate sediments and rocks: New York, Chapman and Hall, 274 p.

Slansky, M., 1986, Geology of sedimentary phosphates: New York, Elsevier, 210 p.

Smith, M.E., Carroll, A.R., and Singer, B.S., 2008, Synoptic reconstruction of a major ancient lake system—Eocene Green River Formation, western United States: Geological Society of America Bulletin, v. 120, p. 54–84.

Sprinkel, D.A., 2009, Interim geologic map of the Seep Ridge 30' x 60' quadrangle, Uintah, Duchesne, and Carbon Counties, Utah, and Garfield and Rio Blanco Counties, Colorado: Utah Geological Survey Open-File Report 549, scale 1:100,000.

Surdam, R.C., and Wolfbauer, C.A., 1975, Green River Formation, Wyoming—a playa-lake complex: Geological Society of America Bulletin, v. 86., p. 335–345.

Taylor, S.R., and McLennan, S.M., 1985, The continental crust—its composition and evolution: London, Blackwell, 312 p.

United States Geological Survey (website, accessed 03 July 2010), USGS geochemical reference materials and certificates: USGS Certificate of Analysis, Green River Shale, SGR-1, http://minerals.cr.usgs.gov/geo_chem_stand/shale.html.

Weiss, M.P., Witkind, I.J., and Cashion, W.B., 1990, Geologic map of the Price 30' x 60' quadrangle, Carbon, Duchesne, Uintah, Utah, and Wasatch Counties, Utah: U.S. Geological Survey Miscellaneous Investigations Series Map I-1981, scale 1:100,000.

Wetzel, R.G., 2001, Limnology—lake and river ecosystems, 3rd Edition: Academic Press, 1006 p.

Witkind, I.J., 1988, Geologic map of the Huntington 30´ x 60´ quadrangle, Carbon, Emery, Grand, and Uintah Counties, Utah: U.S. Geological Survey Miscellaneous Investigations Series Map I-1764, scale 1:100,000.

Witkind, I.J., 1995, Geologic map of the Price 1° x 2° quadrangle, Utah: U.S. Geological Survey Miscellaneous Investigations Series Map I-2462, scale 1:250,000.

Wray, D.S., 1999, Identification and long-range correlation of bentonites in Turonian–Coniacian (Upper Cretaceous) chalks of northwest Europe: Geological Magazine, v. 136, p. 361–371.